SEDIMENTOLOGY
the Journal of the
International Association of Sedimentologists

DEPOSITION AND PRESERVATION OF FLUVIO-TIDAL SHALLOW-MARINE SANDSTONES: A RE-EVALUATION OF THE NEOPROTEROZOIC JURA QUARTZITE (WESTERN SCOTLAND)

Journal:	*Sedimentology*
Manuscript ID	SED-2018-OM-263.R1
Manuscript Type:	Original Manuscript
Date Submitted by the Author:	n/a
Complete List of Authors:	Levell, Bruce; University of Oxford, Department of Earth Sciences Johnson, Howard; Imperial College London, Department of Earth Science and Engineering Collins, Daniel; Imperial College London, Department of Earth Science and Engineering; National Institute of Advanced Industrial Science and Technology Geological Survey of Japan, van Cappelle, Marijn; Imperial College London, Department of Earth Science and Engineering; PDS Group
Keywords:	Tidal, Shelf, Delta, Quartzite, Preservation potential, Proterozoic

DEPOSITION AND PRESERVATION OF FLUVIO-TIDAL SHALLOW-MARINE SANDSTONES: A RE-EVALUATION OF THE NEOPROTEROZOIC JURA QUARTZITE (WESTERN SCOTLAND)

BRUCE K. LEVELL[1*], HOWARD D. JOHNSON[2], DANIEL S. COLLINS[2, 3] and MARIJN VAN CAPPELLE[2,4]

[1]*Department of Earth Sciences, University of Oxford, South Parks Road, Oxford, OX1 3AN UK*

[2]*Department of Earth Science and Engineering, Imperial College London, Prince Consort Road, London, SW7 2BP UK*

[3] *Geological Survey of Japan, AIST, Tsukuba, Japan*

[4] *Petrotechnical Data Systems B.V., Lange Kleiweg 10, 2288 Rijswijk, The Netherlands*

*corresponding author: brucel@earth.ox.ac.uk

ABSTRACT

The 2–5 km thick, sandstone-dominated (>90%) Jura Quartzite is an extreme example of a mature Neoproterozoic sandstone, previously interpreted as a tide-influenced shelf deposit and herein re-interpreted within a fluvio-tidal deltaic depositional model. Three issues are addressed: (1) evidence for the re-interpretation from tidal shelf to tidal delta; (2) reasons for vertical facies uniformity; and (3) sand supply mechanisms to form thick tidal-shelf sandstones. The predominant facies (compound cross-bedded, coarse-grained sandstones) represents the lower parts of metres to tens of metres high, transverse fluvio-tidal bedforms with superimposed smaller bedforms. Ubiquitous erosional surfaces, some with granule–pebble lags, record erosion of the upper parts of those bedforms. There was selective preservation of the higher energy, topographically-lower, parts of channel-bar systems. Strongly asymmetric, bimodal, palaeocurrents are interpreted as due to associated selective preservation of fluvially-enhanced ebb tidal currents. Finer-grained facies are scarce, due largely to suspended sediment bypass. They record deposition in lower-energy environments, including channel mouth bars, between and down-depositional-dip of higher energy fluvio-ebb tidal bars. The lack of wave-formed sedimentary structures and low continuity of mudstone and sandstone interbeds, support deposition in a non-shelf setting. Hence, a sand-rich, fluvial-tidal, current-dominated, largely sub-tidal, delta setting is proposed. This new interpretation avoids the problem of transporting large amounts of coarse sand to a shelf. Facies uniformity and vertical stacking are likely due to sediment oversupply and bypass rather than balanced sediment supply and subsidence rates. However, facies evidence of relative sea level changes is difficult to recognise, which is attributed to (1) the areally extensive and polygenetic nature of the preserved facies, and (2) a large stored sediment buffer that dampened response to relative sea level and/or sediment supply changes. Consideration of preservation bias towards high-energy deposits may be more generally relevant, especially to thick Neoproterozoic and Lower Palaeozoic marine sandstones.

KEYWORDS: Tidal, shelf, delta, quartzite, preservation potential, Proterozoic.

INTRODUCTION

Tidal sandstones are formed in four main depositional settings: (1) tide-dominated deltas (e.g. Goodbred and Saito, 2012; Plink-Björklund, 2012); (2) tide-dominated estuaries (e.g. Dalrymple *et al.,* 1992), (3) tidal inlets (e.g. Hayes and Fitzgerald, 2013); and (4) tide-dominated shelves (e.g. Johnson and Baldwin, 1996; Suter, 2006). Understanding of tide-dominated deltas, estuaries and inlets has recently improved due to extensive studies of Holocene to modern deposits and a better understanding of the influence of relative sea-level fluctuations on shoreline type, morphology, and stratigraphic preservation (e.g. Cattaneo & Steel, 2003; Boyd *et al.,* 2006; Longhitano *et al.,* 2012). In contrast, understanding of tide-dominated shelves and straits (e.g. Pratt, 1990) has lagged behind, complicating their recognition in the rock record. This is succinctly captured by Suter (2006): 'It may be somewhat disquieting to be left with the idea that clastic shelf sands are complex and their identification is not straight forward'.

The tide-dominated shelf model was initially based on the shallow seas of NW Europe (e.g. Stride, 1963; Belderson, 1986; Belderson *et al.,* 1982; Stride *et al.,* 1982). The sand-dominated parts of this area contain a wide range of large-scale, sub-tidal bedforms, including tidal sand waves and sand ridges (e.g. Houbolt, 1968; Stride, 1970; Berné *et al.,* 1994, 1998; Le Bot and Trentesaux, 2004). The resulting depositional process model was applied to laterally-extensive shallow marine sandstones characterized by m-scale cross-stratification ('sand waves') with evidence of bidirectional currents, including thick Proterozoic and Cambrian "quartzite" successions (e.g. Banks, 1973; Anderton, 1976; Levell, 1980). In contrast, modern tidal shelf sand sheets and sand banks have a patchy distribution, are only up to *ca* 10 and 50 m thick, respectively (Stride *et al.,* 1982), show considerable lateral facies variability, and are mostly transgressive sands.

In addition, there are three issues with applying a modern tidal shelf model to thick (*ca* 100s–1000s m), extremely sand-rich (*ca* >80%) laterally and vertically uniform aggradational successions:

(1) How robust is the specific evidence for a tidal shelf interpretation, compared to that for other tidal settings?

(2) What were the depositional and preservational processes responsible for creating an exceptionally thick (up to 5 km) stack of sand-rich facies during kilometers of subsidence?

(3) What were the processes that emplaced large volumes of sand onto the ancient shelf?

The first issue is addressed through detailed facies analysis of high-quality exposures. The second issue, thick successions of uniform facies, is often explained by a persistent balance between rates of accommodation space creation and sediment supply (e.g. Eriksson *et al.*, 1998). However, this "delicate balance" is an unlikely coincidence of fundamentally independent rates (Barrell, 1917). The third issue, of shelf sand supply, is highlighted by comparison of modern and ancient shelf deposits. Modern tide- and storm-dominated shelves show a thin (mainly *ca* 1–10 m; *ca* 40–50 m in tidal sand ridges) and patchy veneer of sand supplied by *in situ* reworking of Quaternary clastic deposits (Swift, 1976; Swift and Thorne, 1991), whereas ancient inferred tidal shelf sandstones are typically several 10's to 100's m thick (e.g. Banks, 1973; Johnson, 1977a and b; McKie, 1990; Abbott and Sweet, 2000) but have been interpreted to reach up to 1,000's m (e.g. Anderton, 1976; Levell, 1980). In general, shoreline to shelf sand transport is inhibited by net onshore transport by shoaling waves ("littoral energy fence"; Allen, 1970; Swift, 1976). Hence, the interpretation of thick sandstones as shelf deposits requires an explanation of how the littoral energy fence was evaded (Levell, 1980).

These issues are addressed through a re-evaluation of the Neoproterozoic Jura Quartzite Formation (Fig. 1). Anderton's (1976) Jura Quartzite depositional model was of an 80 km long NNE-directed tide-dominated shelf sediment transport system.

There were three main reasons for selecting the Jura Quartzite. Firstly, Anderton (1974, 1976) has established a solid facies scheme and regional geological setting. Secondly, the formation represents an extreme example of thickness (*ca* 2–5.2 km) and facies homogeneity (up to 90% coarse-grained sandstone). And thirdly, it is superbly exposed.

REGIONAL GEOLOGICAL SETTING AND PREVIOUS STUDIES

Tectonic and stratigraphic framework of the Jura Quartzite

JURA QUARTZITE

The Jura Quartzite[1] is in the Islay Subgroup of the Argyll Group in the Dalradian Supergroup (Fig. 2), a sequence of metasediments deposited in the Neoproterozoic-Early Cambrian and deformed and folded in the Caledonian (Ordovician) orogeny (Strachan *et al.,* 2002). The Argyll and overlying Southern Highland Groups (Fig. 2) formed the rift to passive margin succession of the north-west side of the Iapetus Ocean (Anderton, 1982; 1985; Strachan *et al.,* 2002; Stephenson *et al.,* 2013). Age constraints are poor (Fig. 2) but the Argyll Group is likely Cryogenian to Ediacaran. There are no absolute dates or even provenance ages (McAteer, 2014) from the Jura Quartzite.

The Argyll Group begins with the Port Askaig Formation, a Neoproterozoic glacial deposit (Spencer, 1971; Ali *et al.,* 2017). This formation contains subordinate quartz-rich tidal sandstones (e.g. Arnaud and Fairchild, 2015), possibly of the same provenance as the succeeding Jura Quartzite. The Port Askaig Formation passes conformably up into the shallow-marine, stromatolite-bearing Bonahaven Dolomite Formation. The contact with the overlying Jura Quartzite is also conformable (but is observed at just one locality: Tanner *et al.,* 2013). The Jura Quartzite is abruptly overlain by the deep-marine Easdale Subgroup, in which mass transport deposits and turbidite sandstones and conglomerates (Scarba Conglomerate; Anderton, 1974) pass gradationally into basinal carbonaceous-rich mudstones (Easdale Slate Formation (Fig 2; Anderton, 1985). The Jura Quartzite to Scarba Conglomerate contact is locally faulted and erosional with slump scars in North

[1] The Jura Quartzite lacks formal formation definition (British Geological Survey website). "Jura Quartzite" is therefore used throughout.

Jura. Further south it is partly transitional with intermediate older, yellow-grey (oxic), and younger, black, slates (“Jura Slate”) below the Scarba Conglomerate (Fig. 2). Overall this suggests a major shelf collapse (Anderton, 1979; 1988).

The Jura Quartzite is *ca* 5.2 km thick in central Jura (Loch Tarbert) and thins along strike to both the SW and NE; the former is attributed to syn-depositional (NE-downthrown) faulting (Islay Transfer Zone, Fig. 3; Anderton, 1985, 1988). In North Jura, the Jura Quartzite also thins to the NE due to both faulting and erosion beneath slump scars (Anderton, 1977, 1979, 1988). The closest down-palaeocurrent equivalents of the Jura Quartzite (40 km to the NE) are thin and poorly known (Benderloch: Litherland, 1980). However correlatives of the Jura Quartzite are known (Strachan and Holdsworth, 2000) in Connemara and Donegal (150 and 300 km to the SW respectively as well as in Perthshire (160 km to the NE). Discussion of these units is beyond the scope of this paper, but clearly the new interpretation of the rocks on Jura as a fluvio-tidal delta rather than as a shelf deposit has implications for the meaning attached to the long-distance correlation of these lithostratigraphic units: e.g. as a continuous near-contemporaneous rock unit or a repeated sequence of depositional conditions in different sub-basins.

Strain-restored thicknesses show that the Argyll Group, including the Jura Quartzite, has a wedge-shape in a NW–SE section across Islay (Fig. 3B; Borradaile, 1979). Hence, the Jura Quartzite was likely deposited in a NE-elongated fault-controlled half-graben *ca* 50 km long and 20 km wide and defined by transfer faults on Islay and near Scarba (Anderton, 1988).

The Jura Quartzite sandstones are sub-arkoses (Anderton, 1974). They often contain pebbles but are only locally conglomeratic. The limited grain size range, compositional maturity and lack of mudstone suggest a second cycle origin (Anderton, 1980) and, probably also the effects of weathering, erosion and transport on non-vegetated land surfaces (e.g. Dott, 2003).

DATASET AND METHODS

This study comprises detailed sedimentary logging, field mapping of bed geometries (20–150 m of selected along-strike exposure) and measurement of palaeocurrents (based on three-dimensional cross-stratification) of the Jura Quartzite based on two large, continuously exposed coastal outcrops: (1) the northern shore of Loch Tarbert, Central Jura (Fig. 1B and C); and (2) the north-western shore of North Jura (Fig. 1B and D). Both sections were studied by Anderton (1974, 1976) and are located *ca* 20 km apart along the inferred sediment transport pathway. This detailed work comprises 850 m of logged stratigraphy, supplemented by observations from Islay, Jura, and Scarba (Fig. 1B). The outcrops are extremely high quality, thanks to exposure on the coastal Main Rock Platform (Sissons, 1979), little structural deformation, and low-grade metamorphism (greenschist facies: although pseudomorphs after kyanite are documented on Islay (Tanner *et al.,* 2013)). Palaeocurrent data have been restored for the bedding dip, with no correction for the larger-scale geometry of the Islay anticline (Borradaile, 1979).

Restoration was based on local dip of major, sharp, planar, (Type 3, see below) erosion surfaces either at the specific interval of interest, or where not immediately available, within 25m stratigraphically.

The Central Jura (Loch Tarbert), study area (1) corresponds to the thickest part of the formation, (2) has high continuity (ca 10 km long and *ca* 50 m wide), and (3) has a mid-depositional-dip position within the formation (Anderton, 1976). Five sections were selected that (Fig. 1C) cover the full stratigraphic and depositional characteristics of this part of the Jura Quartzite, but specifically also contain very subordinate, but distinctive, mudstone interbeds (now cleaved phyllites) that allow the sandstone geometries to be mapped at least on a 1-200m scale.

The North Jura area also has high-quality coastal exposure (Fig. 1D). Two sections were logged in detail: (1) the southern shore of Glentrosdale Bay; and (2) the northern shore of the headland Aird Bhreacain. These were chosen because the thinner-bedded, mudstone-bearing 'fine facies' (Anderton, 1976) are well-developed, much more abundant than in the Central Jura sections and develop into clear coarsening-upward units.

Field mapping and satellite imagery have failed to reveal any distinctive facies changes, unconformities (e.g. candidate sequence boundaries), or transgressive disconformities (e.g. candidate maximum flooding surfaces) that can be traced across the Islay–Jura region. Consequently, the relative stratigraphic positions of the Central and North Jura sections are based on extrapolation by dip and strike, which implies substantial thinning by faulting and/or erosion of the top of the formation in North Jura (Fig. 2).

Depositional setting of the Jura Quartzite: evidence for tidal deposition and the tide-dominated, storm-influenced shelf depositional model

Anderton (1976) proposed a tide-dominated setting for the Jura Quartzite. The principal evidence is bidirectional palaeocurrents measured from all scales of cross-stratification and evident throughout the succession (Fig. 4). However, cross-bed dips are overwhelmingly towards the NE–NW, and mostly very weakly bimodal. Only locally are there abundant palaeocurrents to the SE–SW and/or clearly bimodal bidirectional patterns (e.g. Inner Loch Tarbert and Lussagiven; Figs. 1C, 2).

Other indicators of tidal currents are (1) convex-upward reactivation surfaces in compound cross-bed sets (e.g. Kohsiek & Terwindt, 1981; Boersma & Terwindt, 1981a), (2) dm-scale foresets with periodically-spaced mudstone drapes (Fig. 4C) (e.g. Visser, 1980), (3) sweeping tangential toesets with thick mudstone drapes (‘shovel-shaped’ cross-bedding; e.g. Boersma & Terwindt, 1981b; van den Berg *et al.,* 2007), and (4) interbedded compound cross-bedding on dm-m scales (e.g. Nio and Yang, 1991). Consequently, the evidence for a tide-influenced depositional setting for large parts of the formation is unequivocal.

The dominant northward palaeocurrent trend is accompanied by a NE-fining facies trend, defined by: (1) north-eastwards decrease in maximum and median grain size; (2) north-eastwards decrease in sandstone unit thickness; and (3) higher proportions of fine-grained and interbedded facies in North Jura (25%) compared to *ca* 5% in Central Jura. An increase in 'flagginess' (MacCulloch, 1819; Bailey, 1917) is accompanied by a decrease in mean spacing of sandstone ribs on satellite imagery from *ca* 60 m on Islay to *ca* 25 m on Scarba in the NE (Fig. 1B).

These SW-to-NE facies and palaeocurrent trends were cited as evidence of a tidal shelf sediment transport pathway. This highlighted two contrasting processes (Fig. 18 in Anderton, 1976): (1) tide-dominated conditions prevailed up-depositional-dip (SW) and represented the 'proximal' part of the transport pathway, mainly comprising 'coarse facies'; and (2) storm-dominated processes increased in importance down-depositional-dip (NE) and represented the 'distal' part of the transport pathway, mainly comprising 'fine facies'. The analogue model was partly derived from the shallow seas of NW Europe (Stride, 1963; Kenyon and Stride, 1970; Belderson *et al.,* 1982; Stride et al., 1982) where bedform zones along tidal transport paths are: (1) in equilibrium with present-day shelf processes, but overall are tide-dominated; (2) aligned parallel to mean spring peak near-surface tidal current velocities; and (3) characterised by enhanced sediment transport rates during storm conditions (Stride, 1963; Belderson *et al.,* 1982). Anderton's (1976) model can be classified as a tide-dominated, storm-influenced shelf depositional system (Johnson and Baldwin, 1996).

FACIES ANALYSIS

Overview

The facies nomenclature of Anderton (1974, 1976), based on analyses in Islay, Central and North Jura, and Scarba (Fig. 1B), is retained for this study (Table 1).

'Coarse' facies C comprise white-grey, thick bedded, coarse- to very coarse-grained, sometimes pebbly sandstone with dm-scale cross-beds, often with abundant de-watering structures. Facies C dominates in Central Jura (*ca* 90% by thickness) but decreases in abundance and fines (eventually to medium sand on Scarba) northwards (*ca* 70% by thickness on Scarba; Anderton, 1974).

'Fine' facies F consists of fine- to medium-grained sandstone and mudstone to siltstone. Facies F comprises three subfacies: Laminated 'FL', Rippled 'FR' and Mud 'FM'. Facies F is best developed in North Jura (15% by thickness) and increases northwards.

'Coarse/fine alternations' facies S mostly comprises medium- to thick-bedded, medium- and coarse-grained, cross-bedded sandstone, with occasional granules, interbedded with mudstone and siltstone. Facies S is best developed in North Jura (10%) and near the top of the formation (Inner Loch Tarbert and Lussagiven; Fig. 1C).

Coarse facies (Facies C)

Description

Facies C comprises thick-bedded (Campbell, 1967), dm-scale cross-bedded, very coarse- to coarse-grained, variably sorted sandstone, with scattered granules and small pebbles. Subordinate finer (medium- to coarse-grained) sandstones are often well sorted, whereas the dominant coarser (very coarse to granule) sandstones are moderately sorted and display marked grain size differentiation along and across foresets.

Decimetre cross-bed sets are typically in tabular cosets of climbing or low-angle descending (<10°), compound cosets up to 4 m thick (Fig. 5A; facies CC and CP, (Table 1), Anderton 1974, 1976). Cosets are separated by planar bedding surfaces on various scales (Fig. 6). They often pass down sediment transport direction into single tabular, avalanche sets (*ca* 0.5–1 m thick; Fig. 5B; Anderton's sub facies CB), before reverting, after 5–20 m of down-current migration, into low-angle compound cross-bed cosets (Fig. 7). Palaeocurrents are dominantly towards the north, with subordinate opposed directions (Anderton, 1971, 1976). Bed bases are erosional and beds impersistent over tens of metres due to differential rates of bedform migration.

Soft-sediment deformation structures, resulting from liquefaction and de-watering, are widespread (*ca* 10% of Facies C). The liquefaction anticlines have a spacing of *ca* 2–6 m, which is *ca* 4–6 times the thickness of the liquefied unit. The intervening synclines contain passively deformed cosets. Liquefaction normally affects zones a few tens of metres wide, transitioning laterally, over tens of metres, into undeformed beds.

Interpretation

Facies C represents deposition from transverse sub-aqueous dunes of variable size and complexity (Ashley, 1990). The metre-scale compound cosets preserve large sub-aqueous dunes (‘sand waves’ of Allen, 1980; cf. Allen and Homewood, 1984) with superimposed smaller dunes predominantly migrating downslope. These structures are comparable to dunes and bars in modern sandy braided rivers and macro-tidal environments (e.g. for macro-tidal settings: Dalrymple *et al.,* 1990; Dalrymple and Rhodes, 1995; Martinius and van den Berg, 2011). The occurrence of infrequent, scattered small pebbles suggests that current competence exceeded the maximum grain size available. The weakly bidirectional palaeocurrent patterns, with a predominant NE-direction, support a mixed fluvial-tidal depositional setting.

Liquefaction was localised: bedforms re-formed downstream of liquefied areas and migrated over actively liquefying units, which suggests that the de-watering was a local spatial feature rather than a periodic temporal one.

Fine facies (Facies F)

Description

Anderton (1976) defined three fine subfacies: (1) laminated mudstone (Facies FM) (Fig. 8A); (2) laminated to thin bedded ripple-bedded sandstone and mudstone (Facies FR) (Fig. 8B, C, D); and (3) laminated to thin-bedded plane-laminated sandstone and mudstone (Facies FL) (Fig. 9A–D). (For consistency with Facies C his codes are modified by adding the ‘F’). Importantly, these subfacies are often interbedded on scales of 1–2 m vertically and can be lateral equivalents over 10–20 m.

Facies F sand/mud ratios vary greatly (5–90%). The most mud-rich facies are plane-laminated mudstones with sand laminations, including a distinctive brown (pyritic) mm–cm laminated mudstone (fine facies FM and FL). Sandstone interbeds are medium- to fine-grained. Increasing sand content is manifested as: (1) thin beds of sandstone with lenticular bedding (Reineck and Wunderlich, 1968), often with loaded bases (Facies FR; Fig. 8B); (2) wavy bedding with current ripple cross-lamination or plane-lamination, occasionally amalgamating to form flaser bedding (Facies FR; Fig. 8C), and (3) thin to medium beds of plane-laminated (or rarely sub-dm-scale cross-bedded) medium-grained sandstone (sand-rich Facies FL; Fig. 9). Facies FL displays a spectrum of increasing sand content and bed thickness (Fig. 9), occasionally forming coarsening-upward units. Bed bases are planar to erosional with stepped erosional surfaces and loads and no grading. Top surfaces show rounded ripple crests with 3D linguoid shapes. Sand-filled, irregularly polygonal ‘sub aqueous’ mud cracks occur sporadically.

Beds are laterally discontinuous over 5–15 m: they amalgamate, wedge-out, or thicken, locally even into 5-10 cm cross-bedded medium sandstones. They also on-lap, or sub-crop, dm-deep and several-metre-wide erosional ‘scoops’ (Fig. 8D, 9D). In our study areas, bed length/bed thickness ratios are certainly much lower than those given by Anderton (1974). 5-10 cm thick beds can rarely be followed for 50m.

Interpretation

The predominance of plane-lamination, scarcity of plane-laminated-to-rippled beds and absence of current lineation suggest deposition from suspension under lower flow regime conditions (Howard and Reineck, 1981). The spectrum of bed thickness and sandstone content is interpreted to reflect variations in depositional flow velocities rather than sand availability, given the overall sandiness of the succession.

Facies F is attributed to deposition by lower flow regime bottom traction currents. Abundant mud drapes and wavy to flaser bedding suggest regularly fluctuating flow strengths. The rarity of wave ripple cross-lamination and symmetrical ripples, and the asymmetric bidirectional palaeocurrents, similar to Facies C, suggest a similar fluvio-tidal current regime. The lateral discontinuity, amalgamation and draping bed geometries suggest that currents transported sand over a topographically complex bottom and accelerated and decelerated on length scales of metre to tens of metres. There is no clear evidence of systematic deposition by laterally extensive waning flows or 'event beds'. Load and flame structures indicate thicker, massive mud intervals remained soft after deposition and in some cases may indicate fluid-mud layers.

Coarse/fine alternations facies (Facies S)

Facies S comprise a variable metre-scale interbedding of Facies C and Facies F (Anderton, 1976). There are three distinctive and recurrent combinations (Table 1): (1) A heterolithic cross-bedded subfacies (Facies SH); (2) Interbedded tabular cross-bedded subfacies (Facies ST); and (3) Interbedded gutter-cast and loaded subfacies (Facies SG).

Heterolithic cross-bedded subfacies (Facies SH)

Description

Facies SH comprises 20–50 cm-thick, discontinuous lenses of dm-scale cross-bedded sandstone and interbedded Facies F (Fig. 10). Sandstone beds are: (1) erosionally-based with steep-sided erosional troughs and loading; (2) coarse- to medium-grained with occasional granular lags; (3) lenticular over 5–25 m, frequently with dm-scale discordant onlap relationships between bedsets; and (4) occasionally display dune form-sets or ripples on bed tops. Cross-bedding forms cm–dm-scale single sets or up to 50 cm-thick compound sets and displays: (1) foreset mudstone drapes (Fig. 10A, B), commonly with a regular (cm-scale) spacing; and (2) more variable palaeocurrents compared to Facies C, including southward directions. The Facies F component comprises either mudstone and/or siltstone interbeds or packages of rippled, wavy-bedded, mudstone-draped, thin-bedded fine-grained sandstone.

Interpretation

These cross-bed sets are archetypal of sub-tidal settings (e.g. Martinius and van den Berg, 2011) and are interpreted as three-dimensional transverse bedforms, such as isolated sinuous-crested or lunate dunes. They probably formed under fluctuating flows with complex streamlines, perhaps due to local topographic irregularities. The fine component represents a wide range of bottom current energy.

Interbedded tabular cross-bedded subfacies (Facies ST)

Description

Facies ST consists of alternations of dm-scale tabular sets of planar cross-bedding (Facies CP, Table 1) with mudstone-rich Facies F. Sandstone beds are medium- to occasionally very coarse-grained, sometimes with granules, and form up to 1 m-thick, amalgamated units of 5–20 cm-thick cross-bed sets, lacking liquefaction structures. Interbedded Facies F comprise cm–dm thick pure mudstones or, less commonly, rippled fine sandstones and mudstones.

Interpretation

Facies ST was formed by regularly-sized, straight-crested migrating dunes in a setting with frequent quieter-water conditions that enabled mud deposition. The straight crested dune fields might reflect relatively laterally unrestricted flows, which combined with the granule-grade sediment, suggest local current reworking of Facies C sand. The fine component represents a background of deposition from suspension.

Interbedded gutter-cast and loaded subfacies (Facies SG)

Description

The distinctive features of this subfacies are: (1) 1–30 cm-thick sandstone beds with irregular, stepped erosional bases and gutter-casts, occasionally with ball-and-pillow loading structures; (2) relatively poorly sorted, coarse- to very coarse-grained sandstone, occasionally with granules; and (3) high interbedded mudstone content (10–40% mudstone or siltstone). The 1–30 cm-thick sandstone beds generally extend for just a few metres and are current ripple cross-laminated or plane-laminated, occasionally cross-bedded, and display common mudstone drapes. Rounded linguoid ripples on bed tops show unidirectional cross-lamination. Graded beds are notably rare.

Interpretation

Facies SG was formed by turbulent flows of fluctuating strength that deposited relatively poorly sorted sand over very short distances, possibly containing vertical helical eddies that formed gutter-cast-like structures (Myrow, 1992; Myrow and Southard, 1996; Collins *et al.,* 2017). The anomalously coarse-grained sandstones suggest derivation from winnowed areas. The mudstone component evidences fluctuating current conditions as evidence by the plentiful mudstone drapes.

FACIES ASSOCIATIONS

Five facies associations have been identified: (1) FA-1: Non-sequential cross-bedded liquefied sandstone units; (2) FA-2: Coarsening-upward compound cross-bedded sandstone units; (3) FA-3: Heterolithic compound cross-bedded sandstone units; (4) FA-4: Coarsening-upward mudstone to sandstone facies units; and (5) FA-5: Heterolithic interbedded mudstone and sandstone facies units.

FA-1: Non-sequential cross-bedded liquefied sandstone units

Description

Facies association 1 comprises the bulk of the formation: 2–200 m-thick units of Facies C that are ubiquitous throughout the study area *(ca* ≥70 km along the sediment transport direction; Fig. 1B). Continuous (several tens of metres laterally) erosional bedding planes (Figs. 5C, 6C) divide FA-1 into 2–12 m-thick sub-units (Fig. 11) and were grouped into three types (1–3) by Anderton (1976), which are summarised below with our additional observations.

Type 1 erosion surfaces consist of two styles (1a and 1b). Type 1a comprise a series of shallow scoops, *ca* 2–10 m wide and a few dm to a metre deep, that form bedding surfaces traceable for up to 50 m. Type 1b are set or coset boundaries that comprise lower relief scours overlain by dm-thick sets of cross-bedded sandstones, extend for 10–30 m, and represent the most commonly occurring bedding planes (Figs. 6B and 7).

Type 2 erosion surfaces, described as 'channels' (Anderton, 1976), are up to 2 m deep, several tens of metres wide, and infilled by trough cross-bedded sandstones. In North Jura, they cut down into coarsening-upward units (FA-4). In Central Jura, they comprise nested metre-scale concave-up surfaces that are infilled by onlapping and downlapping sandstones (Fig. 13).

Type 3 erosion surfaces are distinctive ('master') flat bedding planes that extend laterally for at least *ca* 50–100 m with a vertical spacing of *ca* 4–40 m. They display the following features (Figs. 5C, 11, 12): (1) scattered small pebbles; (2) localised (dm-scale) pebble concentrations; (3) continuous pebble lags; (4) mm–cm-thick layers of silty mudstone (Facies CS, Anderton, 1976); and (5) overlying cm–dm-thick heterolithic layers (FA-2).

Interpretation

Facies association 1 could have formed in bedload-dominated fluvial systems or several tide-dominated settings. The asymmetric bimodal palaeocurrent patterns could reflect a combination of (1) the dominance of the NE-flowing currents, and/or (2) the biased preservation of the deposits of NE-directed flows. Equal preservation of bimodal trends in ancient tidal deposits is the exception to the rule (Banks, 1973; Levell, 1980; Bridges, 1982; Harris and Eriksson*,* 1990; Johnson and Levell, 1995; Olariu *et al.,* 2012b). This asymmetry is often attributed to fluvial enhancement of ebb-directed tidal currents, especially in fluvial to tidal transition zones (e.g. Mellere and Steel, 1996; Uličný, 2001; Olariu *et al.,* 2012a; Legler et al, 2013; van Cappelle *et al.,* 2016). Furthermore, in channelised settings, preferential preservation of channel floor or bar-base deposits is likely due to erosion of topographically higher areas. Both factors would contribute to a bias towards seaward-directed palaeocurrents, due to differential preservation of deposits from bedforms that migrated under the strongest, most deeply scouring currents. Maximum seaward-directed sediment transport likely occurred during simultaneous peak fluvial discharge (river floods) and maximum ebb tidal currents (spring tides). Differential preservation of these periods of most rapid bedform migration might also help explain the ubiquitous liquefaction.

Type 1 erosion surfaces form set and coset boundaries and preserve average bedform migration distances. Type 2 erosion surfaces include erosional channels but may also represent infill of pre-existing topographic lows between 2–5 m high bedforms (Fig. 13). The planar nature and geometry of the Type 3 erosion surfaces, especially the pebble lags, are suggestive of persistent sediment winnowing, i.e. high competence currents.

The apparent lack of channel or lateral bar margins, despite the abundant exposure, could be due to large width/depth ratios of channels in tidal deltaic and estuarine settings or a setting where the depositional relief is created by bedform or bar topography rather than channel erosion. The true scale of high-energy, fluvio-tidal channels can only be determined in km-wide, outcrops (Van Wagoner *et al.,* 1990; Wonham and Elliott, 1996; Willis, 2000; Willis and Gabel, 2001, 2003; Yoshida *et al.,* 2004; Legler *et al.,* 2013; van Cappelle *et al.,* 2016). These examples of inferred tide-dominated systems display facies resembling Facies C.

FA-2: Coarsening-upward compound cross-bedded sandstone units

Description

Facies association 2 is significant in demonstrating the scale of genetic units dominated by facies C. It occurs in Central and North Jura and is characterised by two main types of *ca* 2–10 m thick coarsening-upward units dominated by either (1) sigmoidal compound cross-bedding (CU-1; Fig. 14), or (2) or tabular low-angle compound cross-bedding (CU-2; Figs. 11, 12 and 15). These units are bounded by Type 2 and 3 bedding surfaces.

In CU-1, sigmoidal compound cross-bedding consists of large, low-angle (*ca* 5–15°) surfaces that show both tangential toplap and bottomlap against major bedding planes. This subordinate type has only been observed near the top of the formation (Inner Loch Tarbert and Lussagiven; Fig. 1C).

In CU-2, tabular low-angle compound cross-bed contain large-scale, low-angle (<10°) inclined surfaces, comprising laminated medium-coarse sandstone with very thin mudstone and/or siltstone laminae in the lower foresets to bottomsets (facies CP; Figs. 11–14), (including rarely form sets; Fig. 15). The bottomsets pass gradually upwards along the low-angle surfaces into m-scale, tabular cross-bedded very coarse-grained sandstone (e.g. Figs. 12, 13). Two sub-types are recognised (CU-2a and CU-2b).

The CU-2a units are *ca* 4–6 m thick and consist of plane-laminated, medium- to coarse-grained sandstones, which pass upwards through dm- to metre-scale cross-bedded coarse-grained sandstones into very coarse to granule-rich sandstones. Uppermost beds often comprise liquefied dm-scale cosets. These successions terminate with a Type 3 planar bedding plane, occasionally overlain by a lag of granules or small pebbles. The lower *ca* 2 m consists of distinctive thin-bedded parallel laminated medium- to coarse-grained sandstone with interbedded cm-thick mudstones (Fig. 12). The mudstone interbeds pass upwards along low angle inclined surfaces and form tangential bottomsets to 2–4 m thick, compound cosets of Facies C.

The CU-2b units are *ca* 2–8 m thick and consist of coarse- to very coarse-grained sandstone with a basal 20–50 cm-thick thin bedded, medium-grained sandstone unit, and are bounded by Type 3 erosion surfaces (Fig. 5C). Compared with CU-2a, CU-2b units (1) coarsen-upwards more rapidly with a thinner basal finer-grained unit, and (2) contain fewer low-angle surfaces of more limited extent (ca 1 m vertically). Good examples of FA-2 coarsening upward units occur in Central Jura (Figs. 11, 12, 15), they also occur as far up-transport-direction as Southern Islay (Port nan Gallan; Fig. 1B).

Interpretation

Facies association 2 records the migration of various genetically-related, high-relief (>4 m), mainly transverse bedforms (e.g. Allen, 1982; Martinius and van den Berg, 2011). In CU-1, sigmoidal cross-bed sets represent single, m-scale sub-aqueous dunes (Ashley, 1990) or lobate tidal bars (Dalrymple *et al.,* 1990) that formed during high sedimentation rates (Legler *et al.,* 2013). In contrast, CU-2 preserves the down-current migration of large and complex transverse bedforms (*ca* >4 m vertical relief). Smaller sub-aqueous dunes were superimposed on larger-scale bedforms, which resemble ‘sand waves’ (*sensu* Allen, 1980). The upward transition from finer- to coarser-grained sediment was invariably by forward accretion (down sediment transport direction), with just a single example of more lateral current flow where dm sets migrated (Fig. 13E) obliquely across low angle inclined surfaces (Fig. 13D). The occurrence of mudstone in the lower part of tangential foresets and cosets, and the draping of form sets (Fig. 15), indicates bedforms that were in lower energy settings than were normally preserved.

The up to *ca* 10 m-thick coarsening-upward units suggest that the inter-bedform lows were > *ca* 12 m deep. Based on analogous modern environments (e.g. Dalrymple *et al.,* 1990), the preserved successions probably accumulated in water depths *ca* 12–30 m deep. A combination of sediment liquefaction, dewatering-related deformation and winnowing affected the uppermost preserved portions of these bedforms.

FA-3: Heterolithic, compound cross-bedded sandstone units

Description

Facies association 3 has only been observed in the upper 500 m of the formation in Central Jura, where it is closely associated with FA-1 and FA-2 (Fig. 14).

Units are 2–5 m thick, composed of facies C, and display an upwards decrease in mudstone interbeds (Facies FL) and increase in sandstone grain size. The basal parts occasionally include *ca* 0.3–0.5 m-thick mudstone layers that drape scoop-shaped cross-bed sets. The lowermost metre consists of dm-scale, mudstone-draped cross-bed sets that thicken and thin over a few metres, changing laterally from wavy bedded to plane-laminated, coarse-grained sandstone beds. These cross-bed sets amalgamate up-depositional slope into cosets comprising coarser-grained sandstones with fewer mudstone drapes. Compound cosets occur on discontinuous, low angle (*ca* 5º) surfaces. Current ripples and current ripple cross-lamination are rare. Palaeocurrent variability is higher than any other facies association, including more evidence of oppositely-dipping cross-beds.

Interpretation

The bimodal cross-bedding, ubiquitous mudstone drapes and scoop-shaped sets indicate preservation of sub-tidal bars. The increased deposition and/or preservation of flood-oriented sets suggests a reduced fluvial component, which may also explain the lack of pebbles and granules. It is unclear whether the restricted occurrence of FA-3 in the uppermost 500 m of the formation reflects a temporal or a spatial (e.g. axial to lateral) change.

FA-4: Coarsening-upward mudstone to sandstone facies units

Description

Facies association 4 units are 5–30 m thick, pass upwards from mudstone- to sandstone-dominated facies, and are best developed in North Jura and Scarba (Figs. 1D, 16–18). Finer-grained sub-units comprise Facies FR and FL (rippled and plane-laminated) that pass gradationally, but rapidly, upwards into well-sorted, fine- to medium-grained, plane-laminated sandstone sub-units (Facies FL; Fig. 9). These units also thicken-upwards gradationally from sub-cm-scale to dm-scale sandstone interbeds. Plane-laminated sandstone beds display (1) sharp planar bases and tops, (2) occasional stepped erosional bases, (3) rare upward transitions to current ripple cross-lamination, (4) occasional lateral transition (m-scale) into <5º cross-lamination, and (5) absence of grading. Laterally impersistent medium-grained sandstone beds displaying higher-angle cross-stratification, tabular or scoop-shaped, mudstone-draped sets, are occasionally observed. Palaeocurrent trends in cross-bedded facies remain unidirectional towards the NE–NW, with minor SW-oriented directions.

Soft-sediment, dm-scale folds and/or rotated packets of thinly-interbedded sandstone and mudstone above concave-up truncational surfaces, occasionally overlain by minor angular unconformities, are observed in the lower third of FA-4 units. These heterolithic units are 1–2 m thick, cross-bedded and/or with stepped erosional bases (Facies SG) occur unpredictably within FA-4 successions. Minor angular unconformities above syn-depositionally rotated units, which dip more steeply than the tectonic dip, occur in two FA-4 units (one is in Fig. 16; base unit 4).

Several-metre-thick, Facies C units sharply overlie FA-4 units and display large-scale cross-bedding, liquefaction and basal erosional relief (Figs. 16, 17). These Facies C units pass laterally, over several tens of metres, into facies equivalent to the underlying medium-bedded, plane-laminated sandstones of exactly the same facies (FL) as the underlying FA-4 unit.

Interpretation

The coarsening- and thickening-upward trends in FA-4 are attributed to progradation of an active local sediment source into water depths of up to 30 m. The plentiful supply of fine- and medium-grained sand (notably different from Facies C on Jura) was predominantly deposited from suspension in plane laminae without current lineation and also without evidence of wave action (e.g. hummocky cross-stratification or wave ripples). The occasionally observed mudstone-draped foresets, shovel-type cross sets, current ripples and SW–directed palaeocurrents are indications of persistent tidal currents. The dominant unidirectional palaeocurrents suggest strong fluvial influence.

The angular unconformities indicate back-rotation of the now more steeply-dipping beds due to syn-depositional faulting or sliding. This, together with minor slump scars and slump folds, indicates unstable depositional slopes. The succeeding channel incisions, accompanied by a lateral facies transition from channel dunes and bars to plane-lamination, provides strong evidence of a distributary channel mouth-bar system, where suspended sediment, bypassed through the up-depositional-dip Facies C belt, was finally deposited.

FA-5: Heterolithic successions of interbedded mudstone and sandstone facies units

Description

Facies association 5 forms 4–40 m thick, mudstone-rich (*ca* 25%) units comprising a complex interbedding of sandstone and mudstone that lack grain size or bed thickness trends. Facies F and Facies S are dominant, the latter including isolated dm-scale cross-bed sets with concave-up shovel-shaped foreset–bottomsets with mudstone drapes. Form sets, 'herringbone' cross-bed sets and loading into underlying mudstone are also common. Palaeocurrents are variable: dominant NE–NW directions with a wide scatter and persistent, but minor, evidence of reversed currents (Fig. 19).

Sandstone beds are 1–10 cm thick and often display stepped erosional bases (Fig. 10D). They comprise wavy-bedded, current or combined-flow ripple cross-laminated, fine- to medium-grained sandstone with mm- to cm-scale mudstone layers (Fig. 8C). Top surfaces show linguoid current ripples with rounded crests. Bed continuity is low (<10 m), with most beds either amalgamating laterally, downlapping or onlapping one another, or wedging out (Fig. 19). Shallow (dm- to m-scale), 10–20 m wide 'scoops' are ubiquitous and formed either erosionally or, more commonly, constructively by lateral bed thickening and thinning.

Interpretation

Facies association 5 was deposited by bottom traction currents, with bed shear stress around the triple point of dunes, ripples, and lower phase plane beds (Baas *et al.,* 2016). Deposition occurred on a soft mud substrate as shown by loading during bedform migration. Mudstone-draped, bidirectional, scoop-shaped cross-beds reflect bedforms that are common in sub-tidal and fluvio-tidal settings (e.g. van den Berg *et al.,* 2007), where lower-energy conditions were more persistent, maximum current speeds were lower (compared to FA-1 deposition), and current velocity variable over short time scales. The bed geometries imply complex flows with laterally (m-scale) and temporally varying strengths. The variability and more frequent reversals of currents also suggest greater tidal influence, although fluvial and ebb-tide flows continued to dominate. Compared with FA-4, reduced preservation of sand deposited from suspension suggests a lower supply of suspended sand grade sediment. This, together with the lack of granules and pebbles, suggests deposition lateral to, or protected from, the main sediment supply axis.

Facies association 5 could have been deposited in a variety of tidal settings distal and/or lateral to the main fluvial-tidal sediment supply system. Modern analogues might include the northern area of the Fly delta (Dalrymple *et al.,* 2003; Harris *et al.,* 2004; Ogston *et al.,* 2008) or the central area of the Mahakam delta (Allen and Chambers, 1998), where local abandonment was caused by up-river avulsion.

DEPOSITIONAL SYSTEM

Our work confirms the tide-influenced nature of the Jura Quartzite but the following aspects of the depositional system require further evaluation: (1) process and environmental significance of the fine facies; (2) process and environmental significance of the coarse facies; (3) palaeocurrent trends; (4) genetic origin of the coarsening upward facies units; and (5) gross depositional model.

In the tidal shelf model (Anderton, 1976), the distribution of the coarse and fine facies was compared to modern tidal current sediment transport pathways (e.g. Belderson *et al.,* 1982). Fine facies were preferentially deposited in distal parts of these pathways and passed up depositional-dip into a higher-energy zone dominated by larger-scale tidal bedforms (coarse facies). Thin to medium-bedded sandstones within the fine facies were interpreted as due to storm ‘event beds’ preserving a range of proximal (sand-rich) to distal (mud-rich) storm deposits interbedded with post- and inter-storm mudstones.

However, in the areas investigated in this study, beds are normally ungraded, bed continuity is low, lateral facies change common and direct evidence of wave and storm-wave processes is vanishingly small (cf. Harms *et al.,* 1982; Yang *et al.,* 2005; Dumas *et al.,* 2005; Dumas and Arnott, 2006; Yang *et al.,* 2006). Hence, our conclusion is that the fine facies represents a variety of varying-energy deposits, but not shelf storm deposits.

Deposition of the coarse facies was linked to the dominant northwards current flow, representing both the seaward and ebb-tide direction. However, the palaeocurrent asymmetry is too pronounced and persistent to be caused solely by mutually-evasive ebb and flood tidal channels, as occurs in purely tidal systems. Fluvial enhancement of the ebb-tidal current is proposed. Various mechanisms are possible, including a regime of flashy river discharge and hinterland storms. Fluvial enhancement of ebb-tides, as recorded by a dominance of ebb-directed cross-bedding, is common in ancient, progradational, fluvio-tidal deltaic depositional systems (e.g. Willis, 2000; Willis and Gabel, 2001, 2003; Legler *et al.,* 2013, 2014; Chen *et al.,* 2014; Gugliotta *et al.,* 2015; Eide *et al.,* 2016; van Cappelle *et al.,* 2016).

Transport capacity is related to the cube of velocity (Wang, 2012), therefore, the transport of sediment as recorded by the cross-beds in a deposit is a steeply increasing function of current speed, which exaggerates preservation of the strongest currents and amplifies any asymmetry in flow strength. Hence, the observed ebb-plus-fluvial dominance could also reflect a preservational bias towards the higher current energy, topographically lower parts of the fluvio-tidal system. In particular, this could reflect enhanced preservation of channel floor and bar bases (Fig. 12) due to erosion by lateral migration of deep (*ca* 20–30m) channels between bars, which is common in both tide-dominated deltaic and estuarine systems (Allen and Chambers, 1998; Dalrymple *et al.,* 1990, 1992, 2003; Dalrymple and Choi, 2007; Houthuys, 2011; Martinius and van den Berg, 2011). In macrotidal subtidal delta platform settings, such as in front of the present-day Chang Jiang (Yangtze) river mouth, tidal currents may scour up to 50 m deep, which greatly exceeds the erosional depth of rivers (Berné *et al.,* 2002).

Palaeocurrent variability in the Jura Quartzite, including reversed palaeocurrent directions, is not random. Variability is greater in the heterolithic units (Facies S, FA-5) and nearer the top of the formation (Fig. 14A). Flood-tide cross-beds are far fewer and occur in two main forms: (1) dm-thick sets that are interbedded with ebb-directed sets (e.g. Inner Loch Tarbert); and (2) larger avalanche (*ca* 1–2 m thick) and compound sets (Rubin and Hunter, 1983) of descending cross-bedding (*ca* 3–4 m thick) within 4–5 m-thick packages (e.g. Lussagiven, Fig. 14C). The former case reflects closely associated ebb and flood tides of similar strength, while the latter case suggests mutual evasion of ebb and flood tidal bedforms (Robinson, 1960; Sixsmith *et al.,* 2008; Martinius and van den Berg, 2011). Overall, the flood direction was the weaker, and flood-tide-related bedforms developed preferentially in lower-energy settings where slack water mudstone deposition was also more common.

Coarse facies deposition was dominated by transverse tidal bars but only the lower parts of these are preserved (in FA-1–3). Local scour during bedform migration produced ubiquitous low-relief erosion surfaces (Types 1 and 2, Fig. 6B). Broader erosion is manifested in the planar Type 3 bedding surfaces (Figs. 6C, 12, which display occasional top-surface pebble lags and reflect pervasive sediment bypassing, erosion and winnowing. Concave-upward channel margins are likely to have been common in the Jura Quartzite, due to both downcutting erosional processes and constructional bar-related topography. However, their recognition is limited by exposure width and orientation.

The FA-4 units of North Jura (Figs 16,17) are interpreted as fluvial-dominated, tide-influenced distributary channel mouth bars that prograded over finer-grained, more tidally-influenced heterolithic units and were incised by channels with an FA-1 infill. The FA-4 units could resemble elongated mouth bars in the following tide-influenced delta front settings: Fly (Dalrymple *et al.,* 2003), Ganges–Brahmaputra (Kuehl *et al.* 1997, 2005), Chang Jiang (Yangtze; Hori *et al.,* 2001, 2002; Berné *et al.,* 2002), and Mahakam deltas (Allen and Chambers, 1998; Storms *et al.,* 2005).

The delta front/mouth bar interpretation of FA-4 serves to link up-depositional-dip channel and bar facies (FA-1–2) with down-depositional-dip sub-tidal but still current-dominated facies (FA-5).

The termination of Jura Quartzite deposition records a sudden reduction of fluvial sediment input and increased tidal reworking, as evidenced by increased preservation of compound heterolithic bedforms, slack water mudstone and flood-tide deposits in FA-3 (Lussagiven; Fig. 1B). These trends are accompanied by an increase in reworked pebble lags, representing sediment reworking with diminished new fluvial input immediately prior to deposition of the overlying Jura Slate.

Consequently, a fluvial-tidal deltaic depositional setting is proposed for the Jura Quartzite, favouring a sub-tidal, sand-dominated delta platform region of a delta, where there is a lateral coalescence of depositional bars (defining “channels”) and erosional channels (defining “bars”).

DISCUSSION

Three issues concerning the Jura Quartzite were raised at the start of this paper: (1) critically evaluate the evidence for a tidal shelf, estuary or delta depositional system; (2) determine the depositional and preservational controls on *ca* 5 km vertical stacking of sand-rich facies; and (3) address the issue of shelf sand supply.

Question 1: Shelf, estuary, or delta?

Whether the depositional system was part of a shelf, estuary or delta is, in part, a question of definitions. The line at which the mouth of a delta or funnel-shaped estuary becomes the shelf is arbitrary. However, it is difficult to envisage an open shelf, or even the open marine-facing distal part of an embayed shelf, without wave action (cf. Messina et al., 2014), and, in our study areas, the fine facies lack the characteristics of storm-related event beds or specific evidence for wave action.

Much of the fine facies are re-interpreted as being the distal parts of prograding fluvial-tidal mouth bars and the toes of up to ten metre-scale subaqueous transverse dunes; deposition was in a fluvial-tidal current-dominated setting. This is supported by the various facies of prograding mouth bars (FA-4) lacking shelf or shoreface characteristics (e.g. Clifton, 2006; Suter, 2006). Hence, a model is proposed of fluvially-supplied sediment that accumulated in a sub-tidal platform dominated by fluvio-tidal channels, with transverse bedforms and bars, including distributary mouth bars and probably elongate tidal sand ridges (Fig. 20).

Five key observations support a sub-aqueous tide-dominated, delta platform depositional setting (Fig. 20): (1) importance of combined ebb-dominated tidal and fluvial currents; (2) predominance of transverse bedforms over lateral accretion; (3) gross down-depositional-dip fining (i.e. to the NE) within Facies C parallel to the strong asymmetric palaeocurrent trend; (4) clear separation by grain size of bedload material in Facies C (FA-1 and 2) to the SW and suspended load in FA4 to the NE and (5) coarsening-upward mouth bar facies successions in more basinward (NE) locations. Modern sub-tidal delta-front platforms are mantled by a wide range of large tidal bedforms, including elongate sand ridges, and are a common feature of many modern tide-dominated deltas (e.g. Kuehl *et al.,* 1997, 2005; Hori *et al.,* 2001, 2002; Berné *et al.,* 2002; Tanabe *et al.,* 2003; Goodbred and Saito, 2012; Xing *et al.,* 2012; Liu *et al.,* 2013; Xu *et al.,* 2016). Although there is no single modern analogue for the Jura Quartzite depositional setting, one process-based candidate could be the extensive sub-tidal platform in front of the Recent to Modern Chang Jiang (Yangtze) river mouth (Berné *et al.,* 2002). This extensive sand sheet is mantled by tidal sand ridges (up to 26 m high), with both erosional and constructional forms (Berné *et al.,* 2002). Seismically-defined, low-angle (<6°) clinoforms define long-term accretion directions of these large, subaqueous bars and interbar channels. Overall the long axes of these ridges are parallel to the fluvial-/ebb-tide direction and pass gradationally landwards into the modern Chang Jiang (Yangtze) river mouth (Hori *et al.,* 2001, 2002; Berné *et al.,* 2002). However, this modern system has prograded, and retreated, across an open unconfined shelf, which differs significantly from the inferred confined setting of the Jura Quartzite (Anderton, 1985, 1988).

However, specific sub-environments of such modern systems have not been identified by us: namely those formed at higher topographic levels (e.g. inter-tidal flats, bays, lagoons, and emergent bar tops). It is argued that bedload-dominated fluvial-tidal deltas are dominated by a wide facies tract of active, laterally-migrating, channels, which ensure that the preserved deposits are heavily biased towards channel floor sequences (i.e. coarse facies) (Fig. 21). The coarse facies also occupies a substantial along-depositional-dip extent and therefore provides poor control on proximal vs distal position. The lack of clear channel geometries may also argue against such a deltaic setting, but there is reasonable doubt that channels of the likely scale (tens of metres by a km or more) can be identified in the available exposures.

The proposed model for the Jura Quartzite (Fig. 20) implies that an enormous volume of sand was supplied by a sand-rich river system, presumably located further to the SW (largely beyond Islay). It is likely that the extreme sand-richness was a function of the source area. The overall lack of mud and silt may also reflect aeolian deflation of the Neoproterozoic land surface. The scarcity of conglomerate and pebbles, despite the competence of the currents, may well be due to a second cycle origin (i.e. a sandstone-rich drainage area). This sand-richness will also have affected the depositional environment, for example by reducing bank stability and encouraging lateral channel migration of both fluvial and tidal channel systems. The lack of terrestrial and aquatic vegetation may have also impacted weathering processes, hydrodynamic energy conditions and sediment preservation (Bradley *et al.,* 2018).

Question 2: Controls on vertical facies stacking

Thick sequences of a single sedimentary facies association, such as the coarse facies of Central Jura, are sometimes attributed to balance between the rates of volumetric space creation and sediment supply. Some feedback effects between sediment volume (weight) and subsidence can help create a balance for limited periods, for example isostatic compensation or loading of a flowing substrate such as salt (e.g. the Upper Jurassic Fulmar Formation, Central North Sea; Johnson *et al.,* 1986; Howell *et al.,* 1996; Mannie *et al.,* 2014; Wonham *et al.,* 2014). But for base-level-controlled clastic systems, rates of accommodation space creation and sediment supply are independent variables and any balance would be a remarkable coincidence. Thick stacks of uniform facies are more readily explained by an excess of sediment supply over space creation with bypass of the surplus (Barrell, 1917). Type 3 erosion surfaces in the coarse facies, and the segregation of fine- to medium-grained sand in mostly distal, down-transport-path deposits (FA-4), are clear evidence of sediment bypassing. Erosional reworking is evidenced by abundant erosional surfaces and implied by the selective preservation of the coarse facies in the bases of bars and the lower parts of channel fills, as opposed to lower preservation potential deposits formed at higher topographic levels (Fig. 21 B, D, F).

However, to explain the thick and uniform facies stacking, mechanisms are also required that annul or obscure the effects of variations in rates of relative sea level change and sediment supply, which must have occurred over the several million years implied by the accumulation of the Jura Quartzite. It should first however be noted that given a high rate of subsidence, which is likely for a 5km thick homogeneous formation, sea level falls will only result in actual relative sea level falls if the rates of sea level change exceed those of subsidence, and even then will be of reduced duration.

Three attributes of the model of a well-connected fluvial-tidal delta to shallow-marine system (Figs 20, 21) may help provide an explanation: (1) excess sediment supply, (2) a large stored sediment buffer (Holbrook *et al.,* 2006), and (3) responses within the depositional system which may limit facies migration. However, these are all speculative due to inadequate knowledge of dynamic system responses in recent environments.

In high current-energy systems with sub-tidal channels, if sediment supply is in excess of accommodation, sediment will likely be transported further seaward (Fig. 21). In the case of a relative base level fall (Fig. 21C, D), channel incision and increased fluvial gradient may increase this bypassing at the expense of progradation of mouth bars over the shelf. Unfortunately, the ratios of sediment volumes contributing to progradation versus bypass to the shelf as base level changes are not known from recent environments. A new equilibrium of the tidal prism with the aggregate channel cross-sectional area, through vertical and lateral erosion will however be reached (cf. Sambrook-Smith, *et al.* (2010) describing a fluvial channel setting).

Conversely, if there were to be a temporary shortage of sediment supply relative to accommodation (Fig. 21E, F), the fluvial-tidal channels would deepen and the facies belts retreat. However, given an overall excess of sediment supply, this deepening and increase in channel cross-sectional area relative to the tidal prism may simply trigger compensatory aggradation in channels at the expense of some of the sediment by-pass. Furthermore, in a high energy fluvio-tidal system, sediment in the bar / channel complex is potentially available for re-distribution in response to the external change: a sediment buffer (Romans *et al.,* 2016). Speculatively, facies belt retreat might be counteracted or delayed by reworking of sand stored in this sediment buffer, for example into spits protecting sediment-trapping tidal flats and thereby resisting a transgression. Moreover, even if facies belts did retreat, the preferentially preserved deposits (coarse facies in channel and bar bases) would remain similar across the sub-tidal delta platform, although flood-dominated bars (FA-5) and abandoned channels might have a higher representation.

Such a sediment buffer may well of course be eventually overcome. However, the larger the active coarse facies belt (e.g. 10s km along depositional strike and dip in the Jura Quartzite system), and the greater the volume of potentially mobile sediment (between sea level and the composite erosion surface created by the deepest migrating fluvio-tidal channels) the greater the potential to mitigate temporarily-reduced sediment supply. Also, as the higher preservation potential facies (coarse facies) are not particularly diagnostic of water depth, the change in 'balance' between relative sea level and sediment supply may not be recognisable as a facies shift (cf. Tessier *et al.,* 2012). The upper *ca* 50–60 m of the Jura Quartzite (at Lussagiven; Figs. 1B and 14), is the best candidate recognised so far to record a longer-term transgressive period when the sediment buffer was finally depleted.

Question 3: Sand supply to the shelf

The re-interpretation of the thickest parts of this formation as fluvio-tidal deltaic deposits (coalesced fluvial–tidal bars and channels), rather than tidal shelf deposits (amalgamated tidal sand waves), removes the problem of how to supply several km of sand to a continental shelf across the littoral energy fence. Seaward transfer of excess sediment through a delta channel mouth can avoid the barrier of shoreward transport at the littoral energy fence because intra-channel sediment transport occurs at depth (*ca* 10–30 m in the Jura Quartzite system). Such sedimentary systems could be called 'throughput systems' analogous to aeolian dune fields, with deflation of excess sand and large sand buffers in storage within the dune field (Kokurek, 1988, 1999; Bishop, 2007). Candidate modern fluvio-tidal throughput systems are the subtidal delta-front platforms of tide-dominated deltas (Goodbred and Saito, 2012), for example, the present-day Ganges-Brahmaputra (Kuehl *et al.,* 1997, 2005) and Chang Jiang (Yangtze) deltas (Hori *et al*., 2001, 2002; Berné *et al.,* 2002).

CONCLUSIONS

The depositional model of the unusually thick (*ca* 5 km) and extremely sand-rich (*ca* 90%) Neoproterozoic Jura Quartzite has been re-evaluated: a fluvio-tidal, sub-tidal delta platform model is proposed as an alternative to a tide-dominated, storm-influenced tidal shelf depositional setting (Anderton, 1976). The questioning of the previous interpretation was prompted primarily by the lack of evidence for waves, and the poor lateral continuity of beds within even the finest grained mudstone-bearing units. It is supported principally by the discovery of coarsening-upward units interpreted as fluvial-tidal mouth bars in a down-transport-path position in North Jura. This re-interpretation in turn requires the conclusion that there has been a strong preservational bias within the delta system towards high-energy traction current deposits of channel floors and bar bases. This was at the expense of much more environmentally-diagnostic, topographically-higher deposits such as lagoons, tidal flats, bar tops, beaches etc. The resulting deposit is largely composed of essentially ‘residual’ coarser-grained sediment of the fluvio-tidal delta, with finer-grained suspended sediment largely bypassed down-transport-path to the prodelta–shelf and/or slope. A large excess of sediment supply over accommodation space creation, together perhaps with a large sediment buffer of mobile sediment within the delta system, essentially prevented imbalances in external forcing (sediment supply versus relative base level) from resulting in detectable transgressions. Regressions simply generated yet more erosional reworking by active channel migration. Consequently, the result is a stack of very uniform, cross-bedded, coarse-grained sandstone facies over the bulk of the 5 km thickness and the 70 km length of the sediment transport path, as represented by the present-day outcrop of the Jura Quartzite.

ACKNOWLEDGEMENTS

The authors thank the Department of Earth Science and Engineering, Imperial College London for support of DSC and MvC via NERC and Janet Watson PhD scholarships, respectively. We are also grateful for a Geological Society of London Research Grant awarded to DSC and MvC to cover fieldwork costs. Olga Gorbanenko is thanked for her help in the field. We are indebted to the skilled boatmanship provided by Nichol MacKinnon, Sandy Campbell and Alisdair MacLachlan.

REFERENCES

Abbott, S.T. and **Sweet, I. P. (**2000) Tectonic control on third-order sequences in a siliciclastic ramp-style basin: An example from the Roper Superbasin (Mesoproterozoic), northern Australia. *Aust. J. Earth Sci.*, **47**, 637–657.

Ali, D.O., Spencer, A.M., Fairchild, I.J., Chew, K. J. Anderton, R., Levell, B.K., Hambrey, M.J., Dove, A. and **Le Heron, D.P.** (2017) Indicators of relative completeness of the glacial record of the Port Askaig Formation, Garvellach Islands, Scotland. *Precambrian Res*. In press.

Allen, G.P. and **Chambers, J.L.C.** (1998) *Sedimentation in the Modern and Miocene Mahakam Delta*. Indonesian Petroleum Association, Jakarta, 236 pp.

Allen, J.R.L. (1970) *Physical Processes of Sedimentation*. London, Unwin, 248 pp.

Allen, J.R.L. (1980) Sand waves: a model of origin and internal structure. *Sed. Geol.*, **26**, 281–328.

Allen, J.R.L. (1982) Mud drapes in sand wave deposits: a physical model with application to the Folkestone Beds (early Cretaceous, southeast England). *Phil. Trans. Roy. Soc. London A*, **306**, 291–345.

Allen, P.A. and **Homewood, P.** (1984) Evolution and mechanics of a Miocene tidal sand wave. *Sedimentology*, **31**, 63–81.

Anderton, R. (1971) Dalradian palaeocurrents from the Jura Quartzite. *Scott. J . Geol*. **7**, 175–178.

Anderton, R. (1974) Middle Dalradian sedimentation in Argyll with particular reference to the Jura Quartzite, Scarba Conglomerate and Craignish Phyllites. PhD Thesis, Univ. of Reading, 208 pp.

Anderton, R. (1976) Tidal-shelf sedimentation: an example from the Scottish Dalradian. *Sedimentology,* **23**, 429–458.

Anderton, R. (1977) The Dalradian rocks of Jura. *Scott. J. Geol*., **13**, 135–142.

Anderton, R. (1979) Slopes, submarine fans, and syn-depositional faults: sedimentology of parts of the Middle and Upper Dalradian in the SW Highlands of Scotland. In: *The Caledonides of the British Isles – reviewed* (Eds A. L. Harris, C.A.H. Holland and B.E. Leake), *Geol. Soc. London Spec. Publ.*, **8**, 483–488.

Anderton, R. (1980) Distinctive pebbles as indicators of Dalradian provenance. *Scott. J. Geol.,* **16**, 143–152.

Anderton, R. (1982) Dalradian deposition and the late Precambrian–Cambrian history of the North Atlantic region: a review of the early evolution of the Iapetus Ocean. *J. Geol. Soc. London*, **139**, 421–431.

Anderton, R. (1985) Sedimentation and tectonics in the Scottish Dalradian. *Scott. J. Geol*., **21**, 407–436.

Anderton, R. (1988) Dalradian slides and basin development: a radical interpretation of stratigraphy and structure in the SW and Central Highlands of Scotland. *J. Geol. Soc. London,* **145**, 69-78.

Arnaud, E. and **Fairchild I.J.** (2015) The Port Askaig Formation, Dalradian Supergroup, Scotland. In: *The Geological Record of Neoproterozoic Glaciations* (E. Arnaud, G.P. Halverson and G. Shields-Zhou), *Geol. Soc. London Mem*., **36**, 635–642.

Ashley, G.M. (1990) Classification of large-scale subaqueous bedforms; a new look at an old problem. *J. Sed. Petrol.*, **60**, 160–172.

Baas, J.H., Best, J.L. and Peakall, J. (2016) Predicting bedforms and primary current stratification in cohesive mixtures of mud and sand. *J. Geol. Soc*. **173,** 12–25.

Bailey, E.B. (1917) The Islay anticline (Inner Hebrides). *Q. J. Geol. Soc. London,* **72**, 132–164.

Banks, N.L. (1973) Tide-dominated offshore sedimentation, Lower Cambrian, North Norway. *Sedimentology*, **20**, 213–228.

Barrell, J. (1917) Rhythms and the measurement of geological time. *Geol. Soc. Am. Bull.* **28.1,** 745–904.

Belderson, R.H. (1986) Offshore tidal and non-tidal sand ridges and sheets: differences in morphology and hydrodynamic setting. In: *Shelf Sands and Sandstones* (R.J. Knight and J.R. McLean), *Can. Soc. Petrol. Geol. Mem.,* **11,** 293–301.

Belderson, R.H., Johnson, M.A., and **Kenyon, N.H.** (1982) Bedforms. In: *Offshore Tidal Sands – Processes and Deposits* (Ed. A.H. Stride), pp. 27–55. Chapman & Hall, London.

Berné, S., Lericolais, G., Marsset, T., Bourillet, J.-F. and **de Batist, M.** (1998) Erosional offshore sand ridges and lowstand shorefaces: examples from tide- and wave-dominated environments of France. *J. Sed. Res.*, **68**, 540–555.

Berné, S., Trentesaux, A., Stolk, A., Missiaen, T. and de Batist, M. (1994) Architecture and long-term evolution of a tidal sand bank: The Middelkerke Bank (southern North Sea). *Mar. Geol*., **121**, 57–72.

Berné, S., Vagner, P., Guichard, F., Lericolais, G., Liu, Z., Trentesaux, A., Yin, P. and **Yi, H.I.** (2002) Pleistocene forced regressions and tidal sand ridges in the East China Sea. *Mar. Geol.*, **188**, 293–315.

Bishop, P. (2007) Long-term landscape evolution: linking tectonics and surface processes. *Earth Surf. Proc. Land.*, **32**, 329–365.

Boersma J.R. and **Terwindt, J.H.J.** (1981a) Berms on an Intertidal Shoal: Shape and Internal Structure. In: *Holocene Marine Sedimentation in the North Sea Basin* (Eds S.-D. Nio, R.T.E. Schüttenhelm and Tj.C.E. van Weering), *IAS Spec. Publ.* **5**, 39–49. Blackwell Scientific Publications, Oxford.

Boersma J.R. and **Terwindt, J.H.J.** (1981b). Neap-Spring tide sequences of intertidal shoal deposits in a mesotidal estuary. *Sedimentology*, **28**, 151–170.

Borradaile, G.J. (1979) Pre-tectonic reconstruction of the Islay anticline: implications for the depositional history of Dalradian rocks in the SW Highlands In: *The Caledonides of the British Isles – reviewed* (Eds A. L. Harris, C.A.H. Holland and B.E. Leake), *Geol. Soc. London Spec. Publ.*, **8**, 229–238.

Boyd, R., Dalrymple, R.W. and **Zaitlin, B.A.** (2006) Estuarine and Incised-Valley Facies Models. In: *Facies Models Revisited* (Eds H.W. Posamentier and R.G. Walker), *SEPM Spec. Publ.*, 84, 171–235.

Bradley G-M., Redfern J., Hodgetts, D. George A. D., Wach, G.D. Accepted Article (2018) The applicability of modern tidal analogues to pre-vegetation paralic depositional models. *Sedimentology.*

Bridges, P.H. (1982) Ancient offshore tidal deposits. In: *Offshore Tidal Sands – Processes and Deposits* (Ed. A.H. Stride), pp. 172–192. Chapman & Hall, London.

Campbell, C.V. (1967) Lamina, laminaset, bed and bedset. *Sedimentology*, **8**, 7–26.

Cattaneo, A. and **Steel, R.J.** (2003) Transgressive deposits: a review of their variability. *Earth-Sci. Rev.*, **62**, 187–228.

Chen, S., Steel, R.J., Dixon, J.F. and **Osman, A.** (2014) Facies and architecture of a tide-dominated segment of the Late Pliocene Orinoco Delta (Morne L'Enfer Formation) SW Trinidad. *Mar. Petrol. Geol.*, **57**, 208–232.

Collins, D.S., Johnson, H.D., Allison, P.A., Guilpain, P. and **Abdul Zazak, D** (2017) Coupled 'storm-flood' depositional model: Application to the Miocene–Modern Baram Delta Province, north-west Borneo. *Sedimentology*, **64**, 1203–1235.

Clifton H.E. (2006) A reexamination of facies models for clastic shorelines. In *Facies Models Revisited* (Eds R.G. Walker, H. Posamentier), *SEPM, Spec. Publ.*, **84**, pp. 293–338.

Dalrymple, R.W. (1984) Morphology and internal structure of sand waves in the Bay of Fundy. *Sedimentology*, **31**, 365–382

Dalrymple, R.W. and **Choi, K.** (2007) Morphologic and facies trends through the fluvial-marine transition in tide-dominated depositional systems: A schematic framework for environmental and sequence-stratigraphic interpretation. *Earth-Sci. Rev.*, **81**, 135–174.

Dalrymple, R.W. and **Rhodes, R.N.** (1995) Estuarine dunes and bars. In: *Geomorphology and Sedimentology of Estuaries* (Ed. G.M.E. Perillo) pp. 359–422. Elsevier, Amsterdam.

Dalrymple, R.W., Knight, R.J., Zaitlin, B.A. and **Middleton, G.V.** (1990) Dynamics and facies model of a macrotidal sand bar complex. *Sedimentology,* **37**, 577–612.

Dalrymple, R.W., Zaitlin, B.A. and **Boyd, R. (**1992) Estuarine facies models: conceptual basis and stratigraphic implications. *J. Sed. Res.*, **62**, 1130–1146.

Dalrymple, R.W., Baker, E.K., Harris, P. and **Huges, M.G.** (2003) Sedimentology and stratigraphy of a tide-dominated, foreland-basin delta (Fly River, Papua New Guinea). In: *Tropical Deltas of South East Asia — Sedimentology, Stratigraphy and Petroleum Geology* (Eds F.H. Sidi, D. Nummedal, P. Imbert, H. Darman, H.W. Posamentier), *SEPM Spec. Publ.,* **76**, pp. 147–173.

Dempster, T.J., Rogers, G., Tanner, P.W.G., Bluck, B.J., Muir, R.J., Redwood, S.D., Ireland, T.R. and Paterson, B.A. (2002) Timing of deposition, orogenesis and glaciation within the Dalradian rocks of Scotland: Constraints from U–Pb zircon ages. *J. Geol. Soc. London*, **159**, 83–94.

Dott, R.H. (2003) The importance of eolian abrasion in supermature quartzites and the paradox of weathering on vegetation free landscapes. *J. Geol*., **111**, 387–405.

Dumas, S. and Arnott, R.W.C. (2006) Origin of hummocky and swaley cross-stratification— The controlling influence of unidirectional current strength and aggradation rate. *Geology*, **34**, 1073–1076.

Dumas, S., Arnott, R.W.C. and **Southard, J.B.** (2005) Experiments on Oscillatory-Flow and Combined-Flow Bed Forms: Implications for Interpreting Parts of the Shallow-Marine Sedimentary Record. *J. Sed. Res.*, **75**, 501–513.

Eide, C.H., Howell, J.A., Buckley, S., Martinius, A.W., Oftedal, B.T and **Henstra, G.A.** (2016) Facies model for a coarse-grained, tide-influenced delta: Gule Horn Formation (Early Jurassic), Jameson Land, Greenland. *Sedimentology*, **63**, 1474–1506.

Eriksson, P.G., Condie K.C., Tirsgaard, H., Mueller W.U., Altermann W., Miall A.D., Aspler L.B., Catuneanu O. and **Chiarenzelli J.R.** (1998) Precambrian clastic sedimentation systems. *Sed. Geol.*, 120, 5–53.

Fairchild, I.J. (1980) The structure of NE Islay. *Scott. J. Geol*., **16**, 189–197.

Ferrarin, C., Madricardo, F., Rizzetto, F., Mc Kiver, W., Bellafiore, D., Umgiesser, G., Kruss, A., Zaggia, L., Foglini, F., Ceregato, A., Sarretta, A., and **Trincardi, F.** (2018) Geomorphology of scour holes at tidal channel confluences. *J. Geophys. Res.* Earth Surf. 123, 1386-1406.

Ginsberg, S.S., Aliotta, S., and **Lizasoain, G.O.** (2009) Morphodynamics and seismostratigraphy of a deep hole at tidal channel confluence. *Geomorphology*, **104,** 253–261.

Goodbred, S.L. and **Saito, Y.** (2012) Tide-Dominated Deltas. In: *Principles of Tidal Sedimentation* (Eds R.A. Davies and R.W. Dalrymple), pp. 129–149. Springer Science.

Gugliotta, M., Flint, S.S., Hodgson, D.M. and **Veiga** (2016) Recognition criteria, characteristics and implications of the fluvial to marine transition zone in ancient deltaic deposits (Lajas Formation, Argentina). *Sedimentology*, **63**, 1971–2001.

Halliday, A.N., Graham, C.M., Aftalion, M., and **Dymoke, P.,** (1989) The depositional age of the Dalradian Supergroup: U–Pb and Sm–Nd isotopic studies of the Tayvallich Volcanics, Scotland. *J. Geol. Soc., London* **146,** 3–6.

Harms, J.C., Southard, J.B and **Walker, R.G.** (1982) Structures and sequences in clastic rocks. *Soc. Econ. Paleont. Miner. Short Course.* **9,** 249 pp.

Harris, C.W., and **Eriksson, K.A.** (1990) Allogenic controls on the evolution of storm to tidal shelf sequences in the Early Proterozoic Uncompahgre Group, southwest Colorado, USA. *Sedimentology,* **37**, 189–213.

Harris, P.T., Hughes M.G., Baker, E.K., Dalrymple, R.W. and **Keene, J.B.** (2004) Sediment transport in distributary channels and its export to the pro-deltaic environment in a tidally dominated delta: Fly River, Papua New Guinea. *Cont. Shelf Res.*, **24**, 2431–2454.

Hayes, M.O. and **Fitzgerald, D.M.** (2013) Origin, Evolution, and Classification of Tidal Inlets. In: Proceedings, Symposium in Applied Coastal Geomorphology to Honor Miles O. Hayes (Eds T. Kana, J. Michel and G. Voulgaris), *J. Coastal Res. Spec. Issue*, **69**, pp. 14–33.

Holbrook, J.M., and **Bhattacharya, J. (**2012) Reappraisal of the sequence boundary in time and space: case and considerations for an SU (subaerial unconformity) that is not a sediment bypass surface, a time barrier, or an unconformity. *Earth-Sci. Rev.*, **113**, 271–302

Holbrook, J.M., Scott, R.W. and **Oboh-Ikuenobe, F. E.** (2006) Base-level buffers and buttresses: a model for upstream versus downstream control on fluvial geometry and architecture within sequences. *J. Sed. Res.,***76**, 162–174.

Hori, K., Saito, Y., Zhao, Q., Cheng, X., Wang, P., Sato, Y. and **Li, C.** (2001) Sedimentary facies of the tide-dominated paleo-Changjiang (Yangtze) estuary during the last transgression. *Mar. Geol.*, **177**, 331–351.

Hori, K., Saito, Y., Zhao, Q and **Wang, P.** (2002) Architecture and evolution of the tide-dominated Changjiang (Yangtze) River delta, China. *Sed. Geol.*, **146**, 249–264.

Houbolt, J.J.H.C. (1968) Recent sediments in the southern Bight of the North Sea: *Geol. Mijnbouw*, **47,** 245–273.

Houthuys, R. (2011) A sedimentary model of the Brussels Sands, Eocene, Belgium. *Geol. Belgica,* **14***,* 55–74.

Howard, J.D. and **Reineck, H.-E.** (1981) Depositional facies of high-energy beach-to-offshore sequence: comparison with low-energy sequence. *AAPG Bull.*, **65,** 807–830.

Howell, J.A., Flint, S.S. and **Hunt, C.** (1996) Sedimentological aspects of the Humber Group (Upper Jurassic) of the South Central Graben, UK North Sea. *Sedimentology*, **43,** 89–114.

Johnson, H.D. (1977a) Shallow marine sand bar sequences: an example from the late Precambrian of northern Norway. *Sedimentology,* **24,** 245–270.

Johnson, H.D. (1977b) Sedimentation and water escape structures in some late Precambrian shallow marine sandstones from Finnmark, north Norway. *Sedimentology,* **24,** 389–411.

Johnson, H.D. and **Baldwin, C.T.** (1996) Shallow siliciclastic seas. In: *Sedimentary Environments and Facies* (Ed. H.G. Reading), pp. 232–280. Blackwell, Oxford.

Johnson, H. D. and **Levell, B. K.** (1995) Sedimentology of a transgressive, estuarine sand complex: The Lower Cretaceous Woburn Sands (Lower Greensand), southern England. In: *Sedimentary Facies Analysis; A Tribute to the Research and Teaching of Harold G. Reading* (Ed. A. G. Plint). *IAS Spec. Publ.* **22**, pp. 17–46.

Johnson, H.D., Mackay, T.A. and **Stewart, D.J.** (1986) The Fulmar Oil-field (Central North Sea): geological aspects of its discovery, appraisal and development. *Mar. Petrol. Geol.*, **3,** 99–125.

Kenyon, N.H. and **Stride, A.H.** (1970) The tide-swept continental shelf sediments between the Shetland Isles and France. *Sedimentology* **14,** 159–173.

Kocurek, G. (1988) First-order and super bounding surfaces in eolian sequences Bounding surfaces revisited. *Sed. Geol.*, **56**, 193–206.

Kocurek, G. (1999) Aeolian system sediment state: theory and Mojave Desert Kelso dune field example. *Sedimentology,* **46,** 505–515.

Kohsiek, L.H.M. and **Terwindt, J. H. J.** (1981) Characteristics of Foreset and Topset Bedding in Megaripples Related to Hydrodynamic Conditions on an Intertidal Shoal. In: *Holocene Marine Sedimentation in the North Sea Basin* (Eds S.-D. Nio, R.T.E. Schüttenhelm and Tj.C.E. van Weering), *IAS Spec. Publ.* **5**, 27–37. Blackwell Scientific Publications, Oxford.

Kuehl, S.A., Levy, B.M., Moore, W.S. and **Allison, M.A.** (1997) Subaqueous delta of the Ganges-Brahmaputra river system. *Mar. Geol.,* **144**, 81–96.

Kuehl, S.A., Allison, M.A., Goodbred, S.L. and **Kudrass, H.** (2005) The Ganges-Brahmaputra Delta. In: *River Deltas: Concepts, Models, and Examples* (Eds L. Giosan and J.P. Bhattacharya). *SEPM Spec. Publ.,* **83,** pp. 413–434.

Le Bot, S. and **Trentesaux, A.** (2004) Types of internal structure and external morphology of submarine dunes under the influence of tide- and wind-driven processes (Dover Strait, northern France). *Mar. Geol.,* **211,** 143–168.

Legler, B., Johnson, H.D., Hampson, G.J., Massart, B.Y.G., Jackson, C.A., Jackson, M.D., El-Barkooky, A. and **Ravnås, R.** (2013) Facies model of a fine-grained, tide-dominated delta: Lower Dir Abu Lifa Member (Eocene), Western Desert, Egypt. *Sedimentology,* **60**, 1313–1356.

Legler, B., Hampson, G.J., Jackson, C.A., Johnson, H.D., Massart, B.Y.G., Sarginson, M. and **Ravnås, R.** (2014) Facies Relationships and Stratigraphic Architecture of Distal, Mixed Tide- and Wave-Influenced Deltaic Deposits: Lower Sego Sandstone, Western Colorado, U.S.A. *J. Sed. Res.,* **84**, 605–625.

Levell.B.K. (1980) A Late Precambrian tidal shelf deposit: the Lower Sandfjord Formation, Finnmark North Norway. *Sedimentology*, **27**, 539-557.

Litherland, M. (1980) The stratigraphy of the Dalradian rocks around Loch Creran, Argyll. *Scot. J. Geol.*, **16**, 105–23.

Liu, J., Kong, X., Saito, Y., Liu, J.P., Yang, Z. and **Wen, C.** (2013) Subaqueous deltaic formation of the Old Yellow River (AD 1128–1855) on the western South Yellow Sea. *Mar. Geol.,* **344,** 19–33.

Longhitano, S.G., Mellere, D., Steel, R.J. and **Ainsworth, R.B.** (2012) Tidal depositional systems in the rock record: a review and new insights. *Sed. Geol*., **279,** 2–22.

MacCulloch, J. (1819) A Description of the Western Islands of Scotland Including the Isle of Man: Comprising an Account of Their Geological Structure; with Remarks on Their Agriculture, Scenery and Antiquities. Constable, London, 587 pp.

Mannie, A.S., Jackson, C.A-L. and **Hampson, G.J.** (2014) Shallow-marine reservoir development in extensional diapir-collapse minibasins: An integrated subsurface case study from the Upper Jurassic of the Cod terrace, Norwegian North Sea. *AAPG Bull.*, **98**, 2019–2055.

Martinius, A.W. and **van den Berg, J.H.** (2011) Atlas of sedimentary structures in estuarine and tidally-influenced river deposits of the Rhine-Meuse-Scheldt system. EAGE Publications, 298 pp.

McAteer, C.A., Daly, J.S., Flowerdew, M.J., Whitehouse, M.S., and **Monaghan, N.M.** (2014) Sedimentary provenance, age and possible correlation of the Iona Group SW Scotland. *Scot. J. Geol*., **50**, 143–158.

McKie, T. (1990) Tidal and storm influenced sedimentation from a Cambrian transgressive passive margin sequence. *J. Geol. Soc. London,* **147,** 785–794.

Mellere, D. and **Steel, R.J.** (1996) Tidal sedimentation in Inner Hebrides half grabens, Scotland: the Mid-Jurassic Bearreraig Sandstone Formation. In: *Geology of Siliciclastic Shelf Seas* (M. De Batist and P. Jacobs), *Geol. Soc. London Spec. Publ*., **117**, 49–79.

Messina, C., Nemec, W., Martinius, A.W. and Elfenbein, C. (2014) The Garn Formation (Bajocian- Bathonian) in the Kristin Field, Halten Terrace: its origin, facies architecture and primary heterogeneity model. In: From Depositional Systems to Sedimentary Successions on the Norwegian Continental Shelf. (Eds A.W. Martinius, J. Howell, T. Olsen, R. Ravnås, R.J. Steel and J. Wonham), Int. Assoc. Sedimentol. Spec. Publ., 47. 513-550.

Myrow, P.M. (1992) Pot and gutter casts from the Chapel Island Formation, southeast Newfoundland. *J. Sed. Res.*, **62**, 992–1007.

Myrow, P.M. and **Southard, J.B.** (1996) Tempestite deposition. *J. Sed. Res.*, **66,** 992–1007.

Nio, S.-D. and **Yang, C.** (1991) Diagnostic attributes of clastic tidal deposits; a review. In: *Clastic tidal sedimentology* (Eds D.G. Smith, B.A. Zaitlin, G.E. Reinson and R.A. Rahmani). *Can. Soc. Petrol. Geol. Mem.*, **16**, 3–27.

Noble, S.R., Hyslop, E.K. and **Highton, A.J.** (1996) High-precision U-Pb monazite geochronology of the c.806 Ma Grampian Shear Zone and the implications for the evolution of the Central Highlands of Scotland. *J. Geol. Soc. Lond.*, **153**, 511–514.

Ogston, A. S., R. W. Sternberg, C. A. Nittrouer, D. P. Martin, M. A. Goni, and **J. S. Crockett** (2008), Sediment delivery from the Fly River tidally dominated delta to the nearshore marine environment and the impact of El Nino, *J. Geophys. Res.,* **113,** 1–18.

Olariu, C., Steel, R.J., Dalrymple, R.W. and **Gingras, M.K.** (2012a) Tidal dunes versus tidal bars: the sedimentological and architectural characteristics of compound dunes in a tidal seaway, the lower Baronia Sandstone (Lower Eocene), Ager Basin, Spain. In: Modern and Ancient Tidal Depositional Systems: Perspectives, Models and Signatures (Eds S.G. Longhitano, D. Mellere and R.B. Ainsworth), *Sed. Geol. Spec. Issue*, **279**, pp. 134–155.

Olariu, M., Olariu, C., Steel, R.J., Dalrymple, R.W. and **Martinius, A.W.** (2012b) Anatomy of a laterally migrating tidal bar in front of a delta system: Esdolomada Member, Roda Formation, Tremp-Graus Basin, Spain. *Sedimentology*, **59**, 356–378.

Plink-Björklund, P. (2012) Effects of tides on deltaic deposition: Causes and responses. *Sedim. Geol.*, **279**, 107–133.

Pratt, L.J. (1990) The Physical Oceanography of Sea Straits. Springer, 608 pp.

Reineck, H.E. and **Wunderlich, F.** (1968) Classification and origin of flaser and lenticular bedding. *Sedimentology*, **11**, 99–104.

Robinson, A.H.W. (1960) Ebb-flood channel systems in sandy bays and estuaries. *Geography*, **45**, 183–195.

Romans, B.W., Castelltort, S., Covault, J.A., Fildani, A and **Walsh, J.P.** (2016) Environmental signal propagation in sedimentary systems across timescales. *Earth-Sci. Rev.*, **153**, 7–29.

Rooney, A.D., Chew, D.M. and **Selby, D.** (2011) Re–Os geochronology of the Neoproterozoic–Cambrian Dalradian Supergroup of Scotland and Ireland: Implications for Neoproterozoic stratigraphy, glaciations and Re–Os systematics. *Precambrian Res.*, **185**, 202–114.

Rubin, D.M. and Hunter, R.E. 1983 Reconstructing bedform assemblages from compound crossbedding. T.S. Ahlbrandt (Ed.), Aeolian Sediments and Processes, vol. 38, Elsevier, Amsterdam (1983), pp. 407-428

Sambrook Smith, G.H., Best, J.L., Ashworth, P. J., Lane S.N., Parker, N.O., Lunt, I.A. Thomas, R.E. and **Simpson C.J.** (2010) Can we distinguish flood frequency and magnitude in the sedimentological record of rivers? *Geology*, **38**, 579–582.

Sissons, J.B. (1979) The Loch Lomond Stadial in the British Isles. *Nature,* **280**, 199 – 203.

Sixsmith, P.J., Hampson, G.J., Gupta, S., Johnson, H.D. and **Fofana, J.F. (**2008) Facies architecture of a net transgressive sandstone reservoir analog: The Cretaceous Hosta Tongue, New Mexico. *AAPG Bull.*, **92**, 513–547.

Spencer, A. M. (1971) Late Pre-Cambrian glaciation in Scotland. *Geol. Soc. London Mem.,* **6**, 98 pp.

Stephenson, D., Mendum, J.R., Fettes, D.J., and **Leslie, G.** (2013) The Dalradian rocks of Scotland: an introduction. *Proc. Geol. Assoc.,***124**, 3–82.

Storms, J.E.A., Hoogendoorn, R.M., Dam, R.A.C., Hoitink, A.J.F. and Kroonenberg, S.B. (2005) Late Holocene evolution of the Mahakam Delta, east Kalimantan, Indonesia. *Sed. Geol*., **180**, 149–166.

Strachan, R. A. and Holdsworth, R.E. (2000) Late Proterozoic (,750Ma) to Early Ordovician passive margin sedimentation along the Laurentian margin of Iapetus Ch.5, 73-87 In: Woodcock, N.H and Strachan, R.E. (Eds.) Geological History of Britain and Ireland. Blackwells, Oxford, 423pp.

Strachan, R.A., Smith, M., Harris SA.L. and **Fettes, D,J.** (2002) The Northern Highland and Grampian terranes. In: *The Geology of Scotland* (Ed. N.H. Trewin), Geol. Soc. London, pp. 81–148.

Stride, A.H. (1963) Current swept floors near the southern half of Great Britain. *Q. J. Geol. Soc. London*., **119**, 175–199.

Stride, A.H. (1970) Shape and size trends for sand waves in a depositional zone of the North Sea. *Geol. Mag*., **107**, 469–477.

Stride, A.H., Belderson, R.H., Kenyon, N.H. and Johnson, M.H. (1982) Offshore tidal deposits: sand sheet and sand bank facies. In: *Offshore Tidal Sands – Processes and Deposits* (Ed. A.H. Stride), pp. 95–125. Chapman & Hall, London.

Suter J.R. (2006) Facies models revisited: clastic shelves. In: *Facies Models Revisited* (Eds R.G. Walker, H. Posamentier), *SEPM, Spec. Publ*., **84**, pp. 339-397.

Swift, D.J.P. (1976) Continental shelf sedimentation. In: *Marine sediment transport and environmental management* (Eds D.J. Stanley and D.J.P. Swift), pp. 311–350. John Wiley, New York.

Swift, D.J.P. and **Thorne, J.A.** (1991) Sedimentation on Continental Margins, I: A General Model for Shelf Sedimentation. In: *Shelf Sand and Sandstone Bodies: Geometry, Facies and Sequence Stratigraphy* (Eds D.J.P. Swift, G.F. Oertel, R.W. Tillman and J.A. Thorne), pp. 1–31. Blackwell Publishing Ltd.

Tanabe, S., Ta, Thi Kim Oanh, Nguyen, Van Lap, Tateishi, M., Kobayashi, I. and **Saito, Y.** (2003) Delta evolution model inferred from the Holocene Mekong Delta, southern Vietnam. In: *Tropical Deltas of Southeast Asia – Sedimentology, Stratigraphy, and Petroleum Geology* (Eds F.H. Sidi, D. Nummedal, P. Imbert, H. Darman and H.W. Posamentier**),** *SEPM Spec. Publ.*, **76,** pp. 175–188.

Tanner, P.W.G., Bendall, C.A., Pickett , E.A., Roberts J.L., Treagus J.E. and **Stephenson, D.** (2013) The Dalradian rocks of the south-west Grampian Highlands of Scotland. *Proc. Geol. Assoc.,* **124**, 83–147.

Tessier, B., Billeaud, I., Sorrel, P., Delsinne, N. and **Lesueur P.** (2012) Infilling stratigraphy of macrotidal tide-dominated estuaries. Controlling mechanisms and impacts of Holocene climatic changes. The examples of the Seine estuary and the Mont-Saint-Michel Bay, English Channel, NW France. In: *Modern and ancient depositional systems: perspectives, models and signatures* (Eds S.G. Longhitano, D. Mellere, R.B. Ainsworth),. *Sed. Geol. Spec. Issue*, **279**, 62–73.

Uličný, D. (2001) Depositional systems and sequence stratigraphy of coarse grained deltas in a shallow-marine, strike-slip setting: the Bohemian Cretaceous Basin, Czech Republic. *Sedimentology*, **48**, 599–628.

van Cappelle, M., Stukins, S., Hampson, G.J. and **Johnson, H.D.** (2016) Fluvial to tidal transition in proximal, mixed tide-influenced and wave-influenced deltaic deposits: Cretaceous lower Sego Sandstone, Utah, USA. *Sedimentology*, **63**, 1333–1361.

Van den Berg, J.H., Boersma, J.R. and **Van Gelder, A.** (2007) Diagnostic sedimentary structures of the fluvial-tidal transition zone; Evidence from deposits of the Rhine and Meuse. *Geol. Mijnbouw*, **86**, 287–306.

Van Wagoner, J.C., Mitchum, R.M., Campion, K.M. and **Rahmanian, V.D.** (1990) Siliciclastic sequence stratigraphy in well logs, cores, and outcrops: concepts for high-resolution correlation of time and facies: *American Association of Petroleum Geologists Tulsa, Methods in Exploration Series*, No. 7, 55 pp.

Visser, M.J. (1980) Neap-spring cycles reflected in Holocene subtidal large-scale bedform deposits: a preliminary note. *Geology*, **8**, 543–546.

Wang, P. (2012) Principles of sediment transport applicable in tidal environments In: *Principles of Tidal Sedimentology* (Eds R.A. Davis, and R.W. Dalrymple), Springer, pp. 19–34.

Willis, B.J. (2000) Tectonic control of nested sequence architecture in the Sego Sandstone, Neslen Formation and Upper Castlegate Sandstone (Upper Cretaceous), Sevier Foreland Basin, Utah, USA. *Sed. Geol.*, **136**, 277–317.

Willis, B.J. and **Gabel, S.L.** (2001) Sharp-based, tide-dominated deltas of the Sego Sandstone, Book Cliffs, Utah, USA. *Sedimentology*, **48**, 479–506.

Willis, B.J. and **Gabel, S.L.** (2003) Formation of deep incisions into tide-dominated river deltas: implications for the stratigraphy of the Sego Sandstone, Book Cliffs, Utah, U.S.A. *J. Sed. Res.*, **73**, 246–263.

Wonham, J.P. and **Elliott, T.** (1996) High-resolution sequence stratigraphy of a mid-Cretaceous estuarine complex: the Woburn Sands of the Leighton Buzzard area, southern England. In: *Sequence Stratigraphy in British Geology* (Eds S.P. Hesselbo, D.N. Parkinson), *Geol. Soc. London Spec. Publ*., **103**, pp. 41–62.

Wonham, J.P., Rodwell, I., Lein-Mathisen, T. and **Thomas, M.** (2014) Tectonic control on sedimentation, erosion and redeposition of Upper Jurassic sandstones, Central Graben, North Sea. In: *From Depositional Systems to Sedimentary Successions on the Norwegian Continental Margin* (Eds A. W. Martinius, R. Ravnås, J. A. Howell, R. J. Steel, J. P. Wonham), *Int. Assoc. Sedimentol. Spec. Publ*., 46, 473–512.

Xing, F., Wang, Y.P. and **Wang, H.V.** (2012) Tidal hydrodynamics and fine-grained sediment transport on the radial sand ridge system in the southern Yellow Sea. *Mar. Geol.,* **291–294**, 192–210.

Xu, T., Wang, G., Shi, X., Wang, X., Yao, Z., Yang, G., Fang, X., Qiao, S., Liu, S. Wang, X. and **Zhao, Q.** (2016) Sequence stratigraphy of the subaqueous Changjiang (Yangtze River) delta since the Last Glacial Maximum. *Sed. Geol.,* **331,** 132–147.

Yang, B., Dalrymple, R. and Chun, S. (2005) Sedimentation on a wave-dominated, open-coast tidal flat, south-western Korea: summer tidal flat–winter shoreface. *Sedimentology*, **52**, 235–252.

Yang, B., Dalrymple, R.W. and Chun, S. (2006) The significance of hummocky cross-stratification (HCS) wavelengths: Evidence from an open-coast tidal flat, South Korea. *J. Sed. Res.*, **76**, 2-8.

Yoshida, S., Johnson, H.D., Pye, K. and **Dixon, R.J.** (2004) Transgressive changes from tidal estuarine to marine embayment depositional systems: The Lower Cretaceous

Woburn Sands of southern England and comparison with Holocene analogs. *AAPG Bull.*, **88**, 1433–1460.

1354 **TABLE 1**

Name		**Code**	**Description**
Coarse facies		**C**	Coarse- to very coarse-grained cross-bedded sandstone with granules and small pebbles
	Climbing dune cosets	CC	Cosets of tabular cross beds Sets and cosets wedge-out up- and down-transport direction or coalesce into compound sets down-current
	Tabular sets	CP	Sets and cosets of tabular cross beds with planar set and coset boundaries
	Thick tabular sets	CB	Single tabular sets of planar cross bedding
	Trough cosets	CT	Cosets of trough cross beds
	Variably oriented sets	CV	Cosets of planar or trough cross beds of variable orientation
	Sets of low-angle cross bedding	CX	Single sets and cosets of low angle cross-bedding
	Laminated sets	CL	Cosets of parallel laminae
	Silt sets	CS	Blanket, wedge, or lenticular units of siltstone to silty fine-grained sandstone (often green phyllites with spaced cleavage). Included in Facies C only where laterally equivalent to CL in large-scale toesets.
Fine facies		**F**	Thin- to medium-bedded units of interbedded fine- to medium-grained sandstone and mudstone
	Laminated	FL	Cm–dm-thick beds of Parallel and minor cross-laminated fine- to medium-grained sandstone often interbedded with mudstone
	Rippled	FR	Cm–to dm-thick beds of ripple and minor plane-laminated fine- to medium-grained sandstone, typically interbedded with mudstone

	Mud	FM	Massive to laminated mudstone to siltstone with rare interbeds of fine-grained sandstone
Coarse/fine alternations		**S**	Medium- to coarse-grained or occasionally very coarse-grained sandstone interbedded with mudstone
	Heterolithic cross-bedded	SH	Isolated lenticular dm-scale sets of cross-bedded sandstone interbedded with mudstone
	Interbedded tabular cross-bedded	ST	Sets and cosets of tabular cross-bedded sandstone interbedded with mudstone
	Interbedded loaded and gutter cast	SG	Laterally discontinuous (m-scale) sandstone beds (dm-thick) displaying bases with loading and gutter casts, interbedded with mudstone.

Table 1. Facies scheme for the Jura Quartzite from Anderton (1974, 1976) used in this study. For simplicity the subdivisions of the Coarse facies (Facies C), useful in the field, are rarely used in this paper. Three new subdivisions of Facies S are introduced (italicised). See text for detailed descriptions, and process and environment interpretations.

FIGURE CAPTIONS

Fig. 1. (A) Location of the study area in relation to the Dalradian Supergroup province in Scotland. (B) Simplified geological map of the Jura Quartzite in SW Argyll showing the two main study areas (black rectangles): Central Jura and North Jura. (C) Location of studied exposures in Central Jura. (D) Location of studied exposures in North Jura. Refer to Fig. 2 for relative stratigraphic positions of studied exposures.

Fig. 2. (A) Lithostratigraphy of the Dalradian Supergroup in SW Argyll, including available age constraints based on (oldest to youngest): (1) pegmatites and mylonites from the Grampian terrane (U/Pb ages from Noble *et al.,* 1996); (2) organic-rich sediments of the Ballachulish Slate Formation (Re/Os ages from Rooney *et al.,* 2011), and (3) a tuff and a quartz-keratophyre intrusion in the Tayvallich Volcanic Formation (U/Pb ages from Dempster *et al.,* 2002, and Halliday *et al.,* 1989, respectively). (B) A simplified overview log for the Jura Quartzite from Loch Tarbert in Central Jura (Fig. 1C) (from Anderton, 1976). The locations of studied exposures are shown (cf. Fig. 1). The North Jura sections are projected into this log from Central Jura based on strikes from BGS map Sheets 28W (South Jura) and 36 (Kilmartin). Anderton (1977) has demonstrated that the upper part of the Jura Quartzite has been cut-out in North Jura by the Scarba Fault (“SF” Fig. 3) and an erosive slump scar at Kinuachdrachd (Fig. 1D).

Fig. 3. Structural setting of the Jura Quartzite, illustrating the fault-bounded nature of the formation (following Anderton, 1988). (A) A simplified geological map of the Islay–Jura

area, rotated so that the top of the Jura Quartzite is horizontal, making the map an approximate strike section along the SE limb of the Islay Anticline (dip is 10–40º to the SE on Jura). The Jura Quartzite thickens from *ca* 1 km in Southern Islay to *ca* 5 km in Central Jura, probably due to down-faulting towards the NE along syn-depositional "Islay Transfer Zone" (ITZ) faults. Thinning of the Jura Quartzite in North Jura is due to the combined effects of a suspected second transfer fault (not shown, Anderton, 1988) and erosion from above by a major fault and slump scar (SF). (B) Thickening of the Jura Quartzite across the Islay anticline to the NNW (Borradaile, 1979). The geometries are suggestive of an additional, down-to-the-SE normal fault that controlled subsidence. LST= Loch Skerrols Thrust (Borradaile, 1979) BF = Bolsa Fault (Fairchild, 1980).

Fig. 4. Examples of facies evidence for tidal influence (in all photos N or NE is towards the left). (A) Oppositely-dipping cross-bedding superimposed on dm-thick form sets (Facies ST, FA-5). Mudstone partings (mm-scale) appear as recessive cracks (North Jura). (B) Isolated, loaded, flood-oriented (SW) cross-bedding (light grey and white beds at the base of the photo) embedded within cleaved mudstones (top of photo: cleavage planes dip to right). The near vertical stratification in the light grey cross-bed set shows that this subaqueous dune collapsed while migrating over fluid-mud. The overlying whiter sandstone form-set shows NE-dipping cross-lamination (Facies SH, Aird Bhreacain, North Jura; Fig. 1D). (C) Cross-bed sets comprising tangential foresets with multiple mudstone partings and extended toesets in FA-4 (Aird Bhreacain, North Jura; Fig. 1D). (D) Sharp-based, symmetrical-ripple-topped, thin-bedded, medium- to coarse-grained sandstone with interbedded mudstone layers overlain by tabular dm-scale cross-

bedded very coarse-grained sandstone (Facies C, FA 2, Aird Reamhar, Central Jura; Fig. 1C).

Fig. 5. Large-scale scale cross-bedding in Facies C. Major bedding planes are highlighted (in simplistic form) in red and NE-dipping cross-beds in yellow. (A) Single compound coset comprising dm-scale cross-bed sets that are dipping in the same northwards direction as the large-scale, low-angle surfaces (coset boundaries). This structure formed as a result of dm-scale dunes migrating down the lee side of a larger, composite, transverse, subaqueous dune (FA-2, Aird Bhreacain North Jura; Fig. 1C). (B) Multiple sets of simple avalanche cross-beds in very coarse-grained sandstone. This avalanche-style cross-bedding typically passes laterally, within *ca* 20 m, into compound cross-bedding (FA-1, Brein Phort, Central Jura; Fig. 1C). (C) Tabular cosets of dm-scale cross-bedding (lower part of photo), below a Type 3 planar bedding surface (red) with a 4 m-thick composite coset above. The latter structure is interpreted as a single, composite, NE-migrating bedform with smaller superimposed dunes (FA-2, at Aird Reamhar, Central Jura; Figs 1C and *ca* 10 m on Fig 11B).

Fig. 6. Examples of large-scale bedding surfaces in Facies C. (A) Type 1a surface comprising a concave-upwards, scoop-shaped erosional bed boundary, which truncates a major liquefaction anticline at, and below, the notebook. These surfaces are typically overlain by finer-grained deposits, in this case thin-bedded, plane-laminated coarse-grained sandstone and mudstone (Facies FL) (FA-2, Aird Reamhar, Central Jura; Fig.

1C) (B) Type 1b surfaces (red lines) comprising coset boundaries, which are undulatory and can be traced laterally for only several 10s m. Rock bluff in middle distance (pink arrow) is *ca* 8 m high; view is towards the SSE (FA-1, Brein Phort, Central Jura; Fig. 1C). (C) A planar Type 3 surface (red line) with a veneer of small pebbles overlain by a coarsening-upward unit with gently dipping cosets of dm cross-bedded coarse-grained sandstone. Red arrow is a liquefaction structure. View is down dip and towards the SE (Glentrosdale Bay South, North Jura; Fig. 1D).

Fig. 7. Sketch to show the lateral variability in large-scale, cross-bedding styles in Facies C (FA-1) based on logged sections, panoramic photos and palaeocurrent measurements of 63m of section at Brein Phort, Central Jura (Fig. 1C). The base of the section comprises dm-scale sets with reversed dips (blue arrows), which preserve small subaqueous dunes formed under reversed current flow (inferred flood-tide direction). The top of the section contains slightly thicker cross-bed sets, some of which thicken downcurrent and across hanging set boundaries (red dots) into metre-scale angle-of-repose and compound cross-bed sets (cf. Dalrymple, 1984). Palaeocurrents show the strong NE-asymmetry (inferred fluvial/ebb-tide direction). The most laterally-persistent cross-bed sets extend for *ca* 50 m and are associated with smaller-scale (<1 m thick) cross-sets. Liquefaction occurred during bedform progradation: for example, a liquefaction anticline (red triangle) created a depression that was infilled by down-current-prograding dunes shortly after liquefaction.

Fig. 8. Fine facies mudstone (Facies FM) and ripple-laminated (Facies FR) units. (A) Laminated and rippled mudstone (brown) with occasional, isolated sets of dm-scale cross-bedded coarse sandstone (grey). The mudstone to siltstone intervals lack internal lamination, are 30–40 cm thick and are among the thickest observed in this study (Aird Bhreacain, North Jura; Fig. 1D). (B) Rippled fine- to medium-grained sandstone interbedded with mudstone. The current-rippled thin beds display irregular erosional bed bases, small-scale lenticularity and a lack of both grading and amalgamation. Bed bases also occasionally display load and flame structures, with some showing simultaneous ripple migration and loading (FA-5, Glentrosdale Bay South, North Jura; Fig. 1D). (C) Wavy-bedded, current ripple cross-laminated, fine-grained sandstone. Thicker beds show scoured, gutter-like bases and flat tops (Aird Bhreacain, North Jura; Fig. 1D). (D) Medium-grained sandstone unit displaying the typical bundling of plane-laminated and current rippled cross-laminated thin beds. Towards the top right is an example of a scoop-shaped erosion surface (dipping left to right) with onlap, which is suggestive of either bypass by currents or a minor slump scar (FA-4, Glentrosdale Bay South, North Jura; Fig. 1D).

Fig. 9. Plane-laminated fine facies (Facies FL) in FA-4. (A) Thin-bedded, plane-laminated, fine- to medium-grained sandstone with occasional current ripple cross-lamination indicating sediment transport to the right (SW; inferred flood-tide direction) (Glentrosdale Bay South, North Jura; Figs. 1D and 16). (B) Thin-bedded, predominantly plane-laminated medium-grained sandstone, with current ripple cross-lamination and

plane-lamination alternating on a scale of 10–30 mm. Note the lack of grading or discrete event beds. Photographed near the base of the coarsening-upward unit in Fig. 18A (Aird Bhreacain, North Jura; Fig. 1D). (C) The lower part of a 6 m-thick coarsening-upward unit, which is mainly composed of well-sorted, fine- to medium-grained, plane-laminated sandstone beds (Aird Bhreacain, North Jura; Fig. 1D). (D) Scoop-shaped erosional surface (dipping left to right), *ca* 5 m across, with onlapping plane-laminated sandstone, which is characteristic of the lower-to-middle parts of FA-4 coarsening-upward units (Aird Bhreacain, North Jura; Fig. 1D).

Fig. 10. Heterolithic facies (Facies SH) in FA-5. (A) Cross-bedded, medium- and coarse-grained sandstone with mudstone-draped foresets and mudstone interbeds. Note bed and set amalgamation, long toesets and the thicker toeset mudstone drapes. Interbeds comprise current-rippled, fine- to medium-grained sandstones. (B) Typical amalgamation of sets to form a single 50 cm-thick cross-bed set, which gradually pinches out over *ca* 5 m to the left (NE; inferred fluvial/ebb-tide direction). (C) Strongly erosional bases to coarse-grained sandstone beds including micro-loading of rippled thin beds. (D) Loaded bed bases to current-rippled sandstone beds, many of which show simultaneous ripple migration and loading, suggesting migration across a soft mud substrate. All four photographs are from Unit 1 of FA-5 in Fig.16, Glentrosdale Bay South, North Jura (Fig. 1D).

Fig. 11. Stratigraphic stacking patterns and Type 3 erosion surfaces in FA-2 at Aird Reamhar, Central Jura (Fig. 1C). (A) Satellite image (Bing Maps) with the sharp, topographically-defined, periodically-spaced, easterly-dipping Type 3 erosion surfaces (labelled by colours shown in B). The two white boxes define the area of the panoramas in Figs 12 and 13. Palaeocurrent roses, from the intervals between the coloured erosion surfaces, are repeated in those figures. The small circles show the azimuths of isolated paleocurrent observations from other intervals (B) Composite vertical section showing stratigraphic architecture in relation to the Type 3 erosion surfaces (coloured lines), two of which have top-surface winnowed pebble lags (red and pale blue lines at 59 m and 82 m, respectively). The section mostly comprises stacked coarsening-upward units (CU-2b), with a CU-2a unit from 60–73 m (Fig. 12). (C) Spacing of Type 3 surfaces in the logged section.

Fig. 12. (A) Photograph of preserved lower section of large-scale bedform in FA-2 at Aird Reamhar, Central Jura (Fig. 1D; 60–73.5 m in Fig. 11B). (B) Stratigraphic log of FA-2 unit shown in Fig. 12A. Overall, the section consists of two coarsening-upward units (CU-2a) between two sharp, planar Type 3 bedding surfaces (red and black as on Fig. 11). (C) The lower part of the section across the boundary between the two successive coarsening-upward units (65m), each commencing with interbedded medium-grained, plane-laminated sandstone and siltstone that passes up into low-angle, plane-laminated medium-grained beds (Facies CS and CL) and dm-scale cross-beds with palaeocurrents towards the NNW. There is a slight counter-clockwise rotation of

palaeocurrents between the two component sequences. The upper part of the FA-2 units consists of large-scale cross-bedded, very coarse-grained, occasionally granular, sandstones with superimposed 3–5 m-thick composite sets and dewatering structures. (C) Detailed photograph of lower part of FA-2 unit shown in Fig. 12B.

Fig. 13. Bedform migration and erosional geometries in FA-2. The pebble-bearing light blue horizon (in A, B and C) can be correlated as a datum implying that there is 7 m of extra section in this exposure than at the section measured 150 m to the south along the coast (i.e. from 67–81m in Fig. 11B). The exposure photo (A) and sketch (B) are shown with structural dip removed. This shows a downlapping, northward-prograding unit (SSW end of the exposure) above the green surface. A minor coarsening-upward unit (CU-2b) above this downlap surface terminates at a Type 1 bedding surface (5 m in log in C) and is succeeded by cross-bedded coarse-grained sandstone and subordinate interbedded, plane-laminated sandstone. Low-angle surfaces between the green and light blue surfaces have a modal, tilt-corrected, dip of 7° (stereonet in D) and a dominant dip towards the NW (rose diagram in D). Cross-bed dip azimuths from the same interval (E) have a wide dispersion, including some indicating flow lateral to the inclined surfaces. Toward the NNE end of the exposure, the prograding FA-2 units include two nested Type 2 erosion surfaces (black and orange). The black surface passes to the SSW into a non-erosional northward-inclined plane, which downlaps onto the green surface. This suggests that its geometry is due both to constructional relief (SSW) and to erosion (NNE). Aird Reamhar, Central Jura; Fig. 1D.

Fig. 14. Heterolithic, dm-scale bedforms in FA-2 in the uppermost Jura Quartzite at Lussagiven, Central Jura (Fig. 1C). Key to sedimentary structures in Fig 11. (A) Sedimentary log with palaeocurrent measurements indicating bimodal ebb- and flood-tide directions. Coarsening-upward units (CU-1, FA-2) with compound sets of heterolithic cross-bedding with mudstone drapes and bidirectional palaeocurrents occur throughout.. The very top of the Jura Quartzite is marked by an unusually large number of small pebble conglomerate lags (e.g. 60–62 m). (B) Satellite image of the logged section, which is a composite of five segments (numbered 1–5) separated by minor faults and gaps with no exposure. Palaeocurent rose diagram in (A) is derived from segemnts 3, 4 and 5 only and that in C from segment 2 (sketched). (C) Exposure sketch of metre-scale, low-angle, concave up cross-bed sets. Palaeocurrent rose diagram (C) indicates variable and oppositely-dipping trends in cm- to m-scale cross-bed sets. This is consistent with preservation of ebb- and flood-tide-influenced sand bars.

Fig. 15. Large-scale, mudstone-draped, transverse bedform within FA-1. Correlation panel (A) and exposure photograph (B) show inclined bedding planes between two parallel planar surfaces (black below and green above) that define a *ca* 5 m-high migrating bedform. Palaeocurrent azimuths are measured from superimposed dune cross-bedding (C), which are parallel to the dip direction of the low-angle surfaces (5°), indicating that this was a transverse bedform. Rare reverse palaeocurrents to the SW were

measured at the base of the unit. The anomalously thick mudstone-rich unit was possibly deposited as a fluid mud, as evidenced by its massive nature and the sandstone lens (orange) comprising load-balled sandstone. Palaeocurrent patterns from this partly abandoned bedform show bidirectional trends (C). In contrast, palaeocurrent azimuths from laterally adjacent FA-1 sandstones to the South (D) and North (E) of this outcrop, both indicate more unidirectional northerly flow in the inferred active/axial sand-rich transport path (Ruantallain Bothy, Central Jura; Fig. 1C).

Fig. 16. Vertical and lateral stratigraphic stacking patterns illustrating fluvio-tidal mouth bar facies successions (Glentrosdale Bay South, North Jura; Fig. 1D). Key to sedimentary structures in Fig. 11. Stratigraphic logs span a *ca* 55 m-thick succession, which extends laterally for *ca* 150 m. The correlation datum is at the boundary between Units 1 and 2. Beneath this surface, Unit 1 (FA-5) is bounded by two sharp planar Type 3 erosion surfaces, and comprises heterolithic Facies SH and SG, which thicken to the south, implying that either the top or base (more likely the base) is non-horizontal. Unit 2 is fine-grained and comprises thin-bedded sandstone and mudstone of Facies F with both rippled (FR) and plane laminated (FL) beds. A coarsening-upward trend (FA-4) in Unit 3 is vertically and laterally variable, defined by changes from heterolithic deposits (Facies S), through plane-laminated medium-grained sandstone (Facies FL), and into massive liquefied and slumped Facies C. This succession is overlain by local angular unconformities. Unit 4 has a basal planar Type 3 erosion surface and consists of a partially-truncated coarsening-upward unit of plane-laminated sandstone. Note the lateral

discontinuity of cross-bedded (blue), rippled (red), versus plane-laminated (green and orange) facies in Units 1–4. These are not stacks of correlatable waning-flow 'event' beds. Unit 5 (Facies C, FA-1) is an erosionally-based channel sand that laterally thins and passes gradationally into plane-laminated facies (Facies FL; Fig 17B). Unit 6 closely resembles Unit 4 (FA-4) but is erosionally truncated by Unit 7 (Facies C, FA-1). The facies and stratigraphic geometries of Units 3–7 are interpreted as the deposits of a set of prograding fluvio-tidal distributary channel/mouth bar systems.

Fig. 17. Stratigraphic architecture of FA-4 at Glentrosdale Bay South, North Jura (Fig. 1D; cf. Fig. 16). (A) Channelised Facies C sandstone (Unit 5) showing erosional incision into the underlying coarsening-upward succession (Unit 4) (see Fig. 16 for equivalent line drawing). (B) Along strike correlative section *ca* 250 m SW of exposure in A. The white line at the base of the channel is the same as in A and delineates the base of thicker-bedded, plane-laminated, coarse-grained sandstones above the coarsening-upward succession (Unit 4). At this position, the along-strike equivalents of Facies C in channel Unit 7 (Fig. 16) are plane-laminated, medium-grained sandstones (Facies FL) displaying low-angle downlap (red lines). Units 5 and 7 are interpreted as axial channels incising into a laterally-equivalent fluvio-tidal mouth bar. (C) Unit 3 (Fig. 16) comprising the lowermost unit of plane-laminated mudstone and fine-grained sandstones, which coarsens-upward into liquefied and slumped, massive, medium-grained sandstone. (D) Plane-laminated Facies FL in Unit 4, which, to the NE, are incised by Unit 5 (Figs. 16 and 17A).

Fig. 18. Stratigraphic architecture and relationships of FA-4 and FA-5 at Aird Bhreacain, North Jura (Fig. 1D). (A) Stratigraphic log with palaeocurrent measurements from Facies S (blue). (B) Exposure photograph of part of the *ca* 25 m thick coarsening- and thickening-upward unit predominantly consisting of (bottom to top): (1) fine-grained, ripple-cross-laminated sandstones (red in A); (2) plane-laminated thin- to medium-bedded medium-grained sandstone (green in A) with heterolithic cross-bedded facies (blue in A); and (3) liquefied coarse-grained sandstone (Facies C, white in A). (C) Exposure photograph of part of the underlying FA-5 units, predominantly comprising heterolithic facies in the toesets of large-scale bedforms. These facies and stratigraphic characteristics suggest that the FA-4 unit prograded over the FA-5 unit, and are consistent with a fluvio-tidal channel/mouth bar prograding over the toes of a sub-tidal bedform. Facies key as in Fig. 16.

Fig 19. Stratigraphic architecture of FA-5 at Inner Loch Tarbert (A) and Lussagiven (B) (3 m in Fig. 14A), Central Jura (Fig. 1C). Decimetre-thick bedsets of mudstone-draped cross-bed sets are interbedded with plane-laminated and occasionally current ripple cross-laminated thin-bedded sandstones and mudstones. Progradation directions of cross-bed sets (red arrows) display frequent current reversals. Individual units are defined by through-going, metre-scale bedding planes (white). Heterolithic units occasionally form low-angle (5°) compound cosets.

Fig. 20. Depositional model for the Jura Quartzite consisting of a sand-rich fluvio-tidal delta platform dominated by laterally migrating channels with intervening fluvio-tidal

bars connected up-depositional-dip to active river systems (AR) ('on-axis'). Lateral embayment areas of decreased sediment supply, adjacent to inactive river systems (IR), include tidal sand ridges or elongate bars ('off-axis') and have more tidal characteristics. Delta progradation and abandonment is largely controlled by upstream avulsion. The predominant coarse facies mostly preserves channel floor deposition that occupies a substantial along transport path extent.

Fig. 21. River-to-shelf cross-sections (approximately 60–70 km NE–SW in the Jura Quartzite), showing high tide (HT) and low tide (LT), and schematic barform morphology and stratigraphy resulting from active channel migration. The lower limit of the cross-sections is an arbitrary 'Regional Composite Scour' surface (Holbrook and Bhattacharya, 2012) that represents erosion by the deepest fluvio-tidal channels (perhaps up to 30–50 m at tidal channel confluences: Ginsberg *et al.,* 2009; Ferrarin *et al.,* 2018). The sections are presented in pairs (A,B), (C,D) and (E,F) with the upper showing facies and the lower preservation potential. (A) The coarse facies (in FA-1,-2,-3 and -5) is in yellow, with inferred proximal alluvial equivalents in orange. The delta-front units (brown) include the predominantly fine facies FA-4 units. The "pro-delta shelf" facies are inferred distal equivalents. (B) As in A but indicating variable preservation potential. The upper limit of high preservation potential (blue) is shown as an arbitrary depth below sea level related to the efficacy of lateral erosion by migrating fluvio-tidal channels, which in reality will vary spatially and temporally. Facies above this level (e.g. bar tops, intertidal deposits, etc.) are selectively removed and are assigned a low preservation potential (red); this sediment is in 'temporary' storage. Excess sediment bypass is indicated by the

horizontal grey arrow. (C) As in A but with falling relative base level. Channel incision and increased fluvial gradient increase sediment bypass (grey arrow). There is some mouth bar progradation. (D) As in C but indicating the change in preservation potential related to the relative base level fall. Channel floor deposits are selectively preserved. (E) As in A but with rising relative base level. Sediment bypass is reduced (grey arrow), but an excess of sediment supplied relative to accommodation space is argued for the Jura Quartzite system. The large volume of sediment stored in the fluvio-tidal delta bars provides a ‘sediment buffer’ whose re-shaping through internal environmental dynamics could, speculatively, counteract transgression-driven facies belt shifts (e.g. Romans *et al.,* 2016). (F) As in E but indicating the change in preservation potential related to the relative base level rise. Channel floor deposits are again selectively preserved, but the preservation boundary aggrades to include shallower bar flanks.

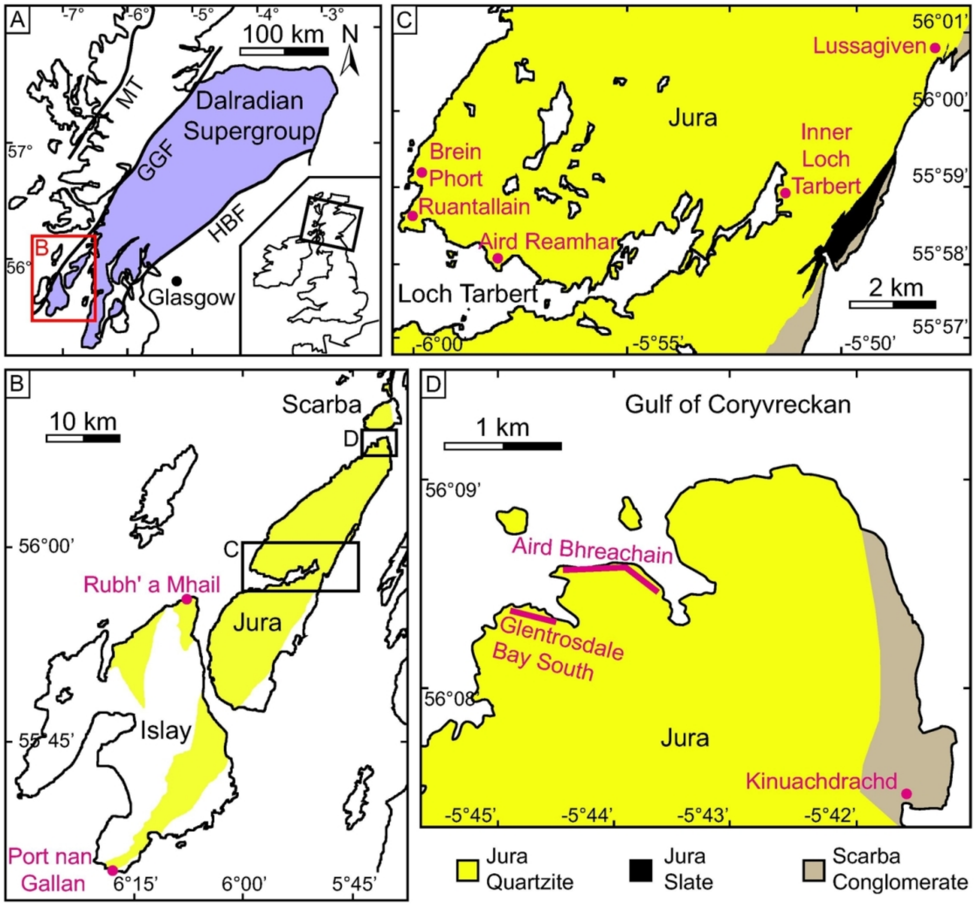

Fig. 1. (A) Location of the study area in relation to the Dalradian Supergroup province in Scotland. (B) Simplified geological map of the Jura Quartzite in SW Argyll showing the two main study areas (black rectangles): Central Jura and North Jura. (C) Location of studied exposures in Central Jura. (D) Location of studied exposures in North Jura. Refer to Fig. 2 for relative stratigraphic positions of studied exposures.

124x114mm (300 x 300 DPI)

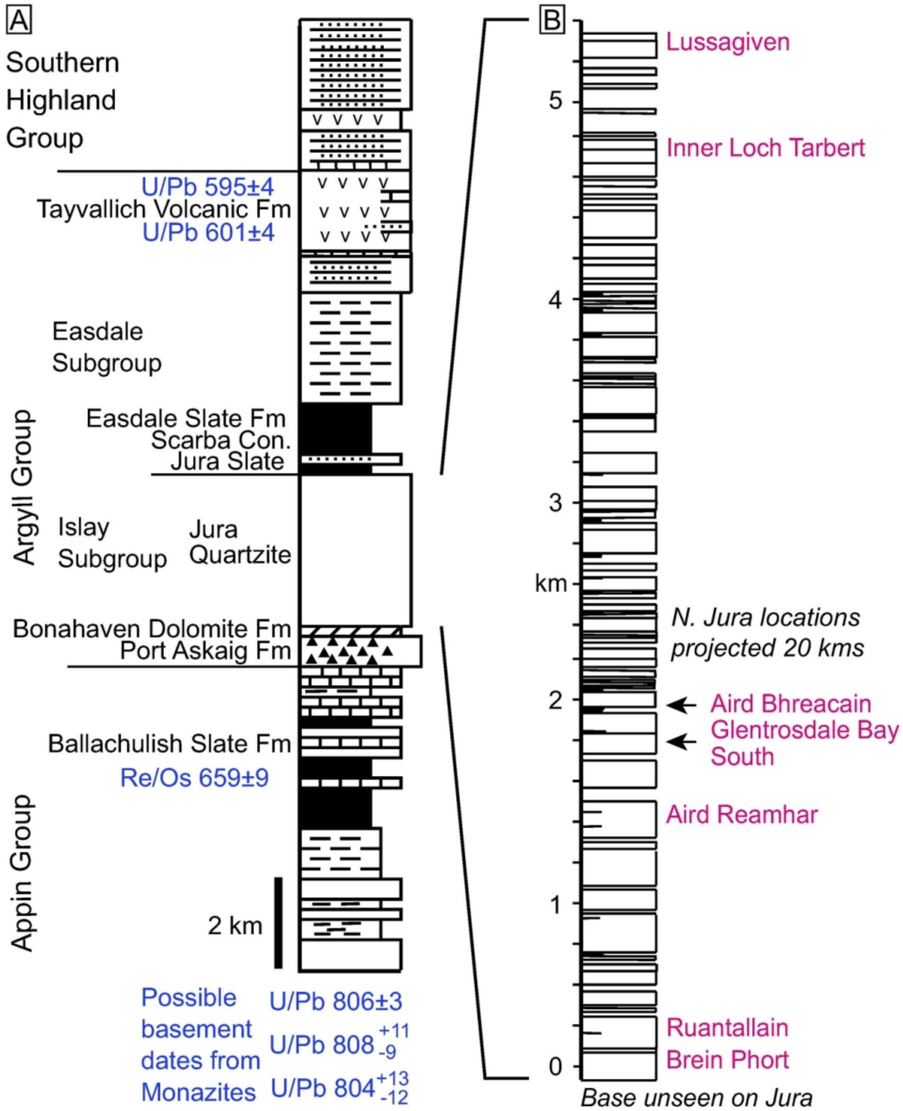

Fig. 2. (A) Lithostratigraphy of the Dalradian Supergroup in SW Argyll, including available age constraints based on (oldest to youngest): (1) pegmatites and mylonites from the Grampian terrane (U/Pb ages from Noble et al., 1996); (2) organic-rich sediments of the Ballachulish Slate Formation (Re/Os ages from Rooney et al., 2011), and (3) a tuff and a quartz-keratophyre intrusion in the Tayvallich Volcanic Formation (U/Pb ages from Dempster et al., 2002, and Halliday et al., 1989, respectively). (B) A simplified overview log for the Jura Quartzite from Loch Tarbert in Central Jura (Fig. 1C) (from Anderton, 1976). The locations of studied exposures are shown (cf. Fig. 1). The North Jura sections are projected into this log from Central Jura based on strikes from BGS map Sheets 28W (South Jura) and 36 (Kilmartin). Anderton (1977) has demonstrated that the upper part of the Jura Quartzite has been cut-out in North Jura by the Scarba Fault ("SF" Fig. 3) and an erosive slump scar at Kinuachdrachd (Fig. 1D).

124x139mm (300 x 300 DPI)

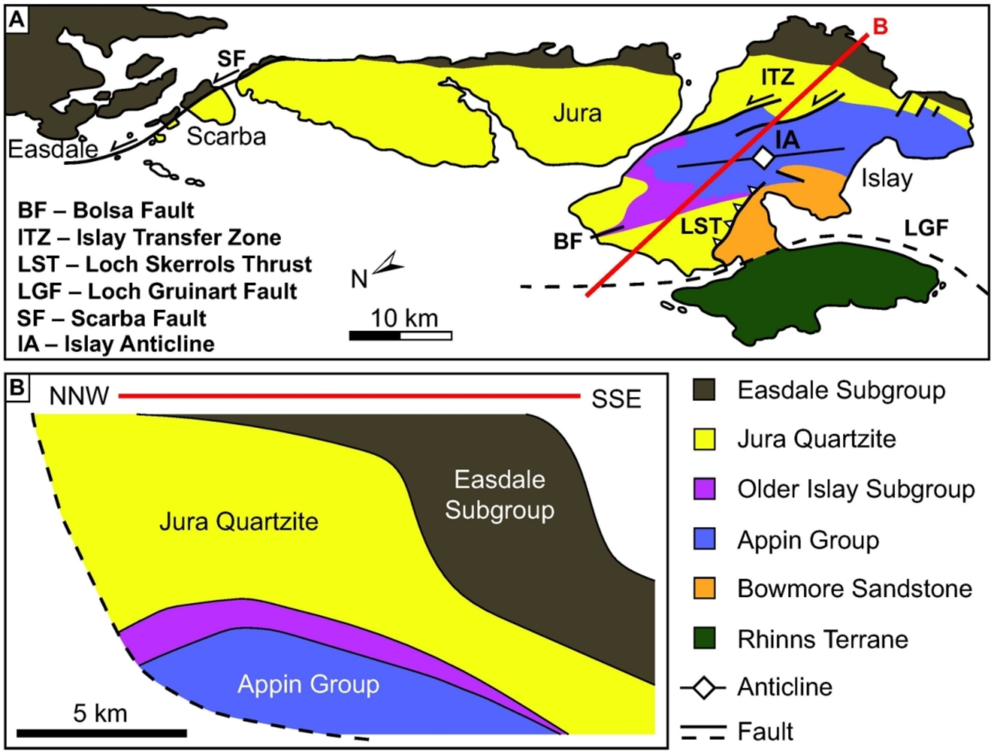

Fig. 3. Structural setting of the Jura Quartzite, illustrating the fault-bounded nature of the formation (following Anderton, 1988). (A) A simplified geological map of the Islay–Jura area, rotated so that the top of the Jura Quartzite is horizontal, making the map an approximate strike section along the SE limb of the Islay Anticline (dip is 10–40º to the SE on Jura). The Jura Quartzite thickens from ca 1 km in Southern Islay to ca 5 km in Central Jura, probably due to down-faulting towards the NE along syn-depositional “Islay Transfer Zone” (ITZ) faults. Thinning of the Jura Quartzite in North Jura is due to the combined effects of a suspected second transfer fault (not shown, Anderton, 1988) and erosion from above by a major fault and slump scar (SF). (B) Thickening of the Jura Quartzite across the Islay anticline to the NNW (Borradaile, 1979). The geometries are suggestive of an additional, down-to-the-SE normal fault that controlled subsidence. LST= Loch Skerrols Thrust (Borradaile, 1979) BF = Bolsa Fault (Fairchild, 1980).

124x95mm (300 x 300 DPI)

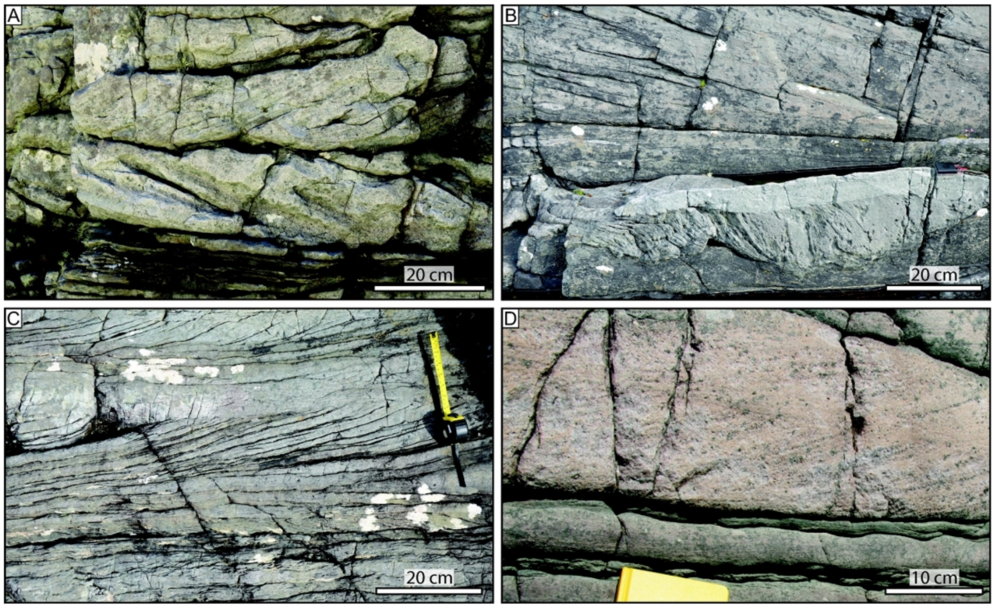

Fig. 4. Examples of facies evidence for tidal influence (in all photos N or NE is towards the left). (A) Oppositely-dipping cross-bedding superimposed on dm-thick form sets (Facies ST, FA-5). Mudstone partings (mm-scale) appear as recessive cracks (North Jura). (B) Isolated, loaded, flood-oriented (SW) cross-bedding (light grey and white beds at the base of the photo) embedded within cleaved mudstones (top of photo: cleavage planes dip to right). The near vertical stratification in the light grey cross-bed set shows that this subaqueous dune collapsed while migrating over fluid-mud. The overlying whiter sandstone form-set shows NE-dipping cross-lamination (Facies SH, Aird Bhreacain, North Jura; Fig. 1D). (C) Cross-bed sets comprising tangential foresets with multiple mudstone partings and extended toesets in FA-4 (Aird Bhreacain, North Jura; Fig. 1D). (D) Sharp-based, symmetrical-ripple-topped, thin-bedded, medium- to coarse-grained sandstone with interbedded mudstone layers overlain by tabular dm-scale cross-bedded very coarse-grained sandstone (Facies C, FA 2, Aird Reamhar, Central Jura; Fig. 1C).

169x104mm (300 x 300 DPI)

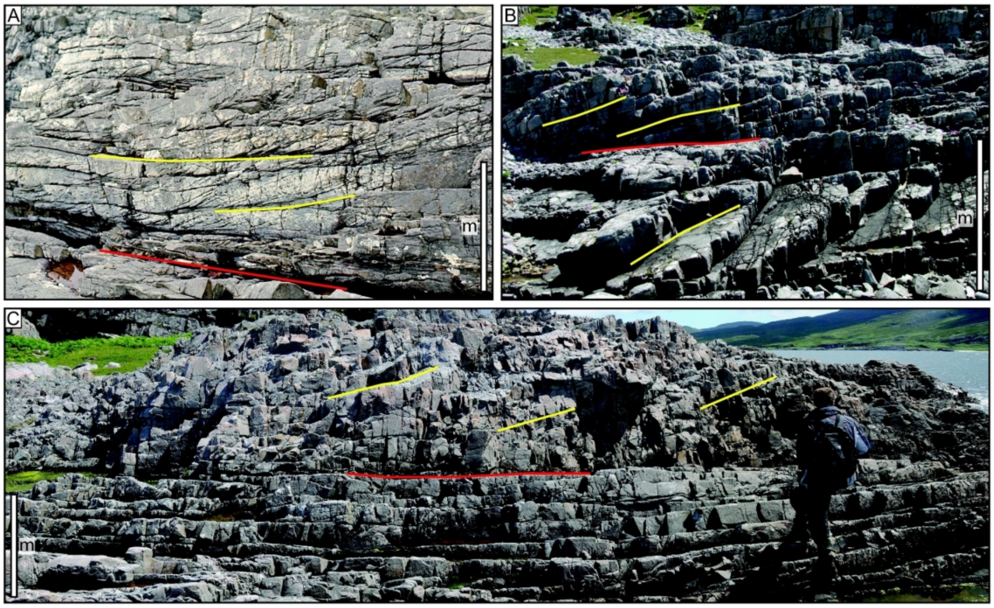

Fig. 5. Large-scale scale cross-bedding in Facies C. Major bedding planes are highlighted (in simplistic form) in red and NE-dipping cross-beds in yellow. (A) Single compound coset comprising dm-scale cross-bed sets that are dipping in the same northwards direction as the large-scale, low-angle surfaces (coset boundaries). This structure formed as a result of dm-scale dunes migrating down the lee side of a larger, composite, transverse, subaqueous dune (FA-2, Aird Bhreacain North Jura; Fig. 1C). (B) Multiple sets of simple avalanche cross-beds in very coarse-grained sandstone. This avalanche-style cross-bedding typically passes laterally, within ca 20 m, into compound cross-bedding (FA-1, Brein Phort, Central Jura; Fig. 1C). (C) Tabular cosets of dm-scale cross-bedding (lower part of photo), below a Type 3 planar bedding surface (red) with a 4 m-thick composite coset above. The latter structure is interpreted as a single, composite, NE-migrating bedform with smaller superimposed dunes (FA-2, at Aird Reamhar, Central Jura; Figs 1C and ca 10 m on Fig 11B).

169x104mm (300 x 300 DPI)

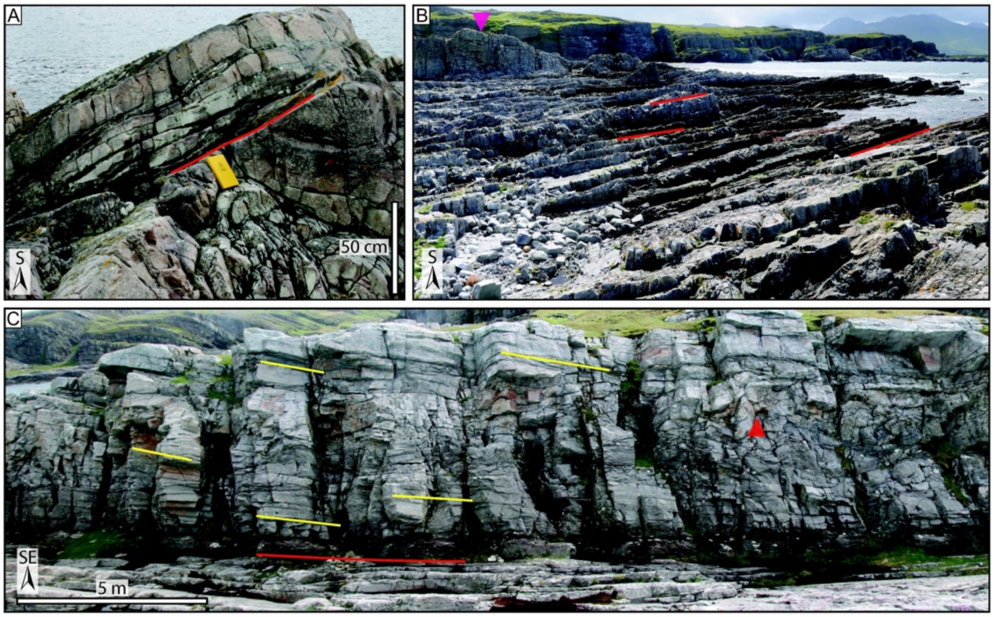

Fig. 6. Examples of large-scale bedding surfaces in Facies C. (A) Type 1a surface comprising a concave-upwards, scoop-shaped erosional bed boundary, which truncates a major liquefaction anticline at, and below, the notebook. These surfaces are typically overlain by finer-grained deposits, in this case thin-bedded, plane-laminated coarse-grained sandstone and mudstone (Facies FL) (FA-2, Aird Reamhar, Central Jura; Fig. 1C) (B) Type 1b surfaces (red lines) comprising coset boundaries, which are undulatory and can be traced laterally for only several 10s m. Rock bluff in middle distance (pink arrow) is ca 8 m high; view is towards the SSE (FA-1, Brein Phort, Central Jura; Fig. 1C). (C) A planar Type 3 surface (red line) with a veneer of small pebbles overlain by a coarsening-upward unit with gently dipping cosets of dm cross-bedded coarse-grained sandstone. Red arrow is a liquefaction structure. View is down dip and towards the SE (Glentrosdale Bay South, North Jura; Fig. 1D).

170x106mm (300 x 300 DPI)

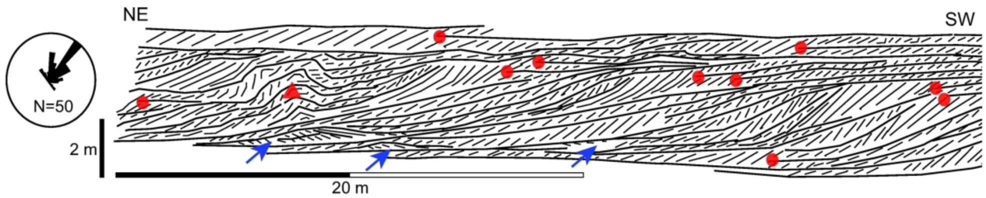

Fig. 7. Sketch to show the lateral variability in large-scale, cross-bedding styles in Facies C (FA-1) based on logged sections, panoramic photos and palaeocurrent measurements of 63m of section at Brein Phort, Central Jura (Fig. 1C). The base of the section comprises dm-scale sets with reversed dips (blue arrows), which preserve small subaqueous dunes formed under reversed current flow (inferred flood-tide direction). The top of the section contains slightly thicker cross-bed sets, some of which thicken downcurrent and across hanging set boundaries (red dots) into metre-scale angle-of-repose and compound cross-bed sets (cf. Dalrymple, 1984). Palaeocurrents show the strong NE-asymmetry (inferred fluvial/ebb-tide direction). The most laterally-persistent cross-bed sets extend for ca 50 m and are associated with smaller-scale (<1 m thick) cross-sets. Liquefaction occurred during bedform progradation: for example, a liquefaction anticline (red triangle) created a depression that was infilled by down-current-prograding dunes shortly after liquefaction.

169x35mm (300 x 300 DPI)

Fig. 8. Fine facies mudstone (Facies FM) and ripple-laminated (Facies FR) units. (A) Laminated and rippled mudstone (brown) with occasional, isolated sets of dm-scale cross-bedded coarse sandstone (grey). The mudstone to siltstone intervals lack internal lamination, are 30–40 cm thick and are among the thickest observed in this study (Aird Bhreacain, North Jura; Fig. 1D). (B) Rippled fine- to medium-grained sandstone interbedded with mudstone. The current-rippled thin beds display irregular erosional bed bases, small-scale lenticularity and a lack of both grading and amalgamation. Bed bases also occasionally display load and flame structures, with some showing simultaneous ripple migration and loading (FA-5, Glentrosdale Bay South, North Jura; Fig. 1D). (C) Wavy-bedded, current ripple cross-laminated, fine-grained sandstone. Thicker beds show scoured, gutter-like bases and flat tops (Aird Bhreacain, North Jura; Fig. 1D). (D) Medium-grained sandstone unit displaying the typical bundling of plane-laminated and current rippled cross-laminated thin beds. Towards the top right is an example of a scoop-shaped erosion surface (dipping left to right) with onlap, which is suggestive of either bypass by currents or a minor slump scar (FA-4, Glentrosdale Bay South, North Jura; Fig. 1D).

169x104mm (300 x 300 DPI)

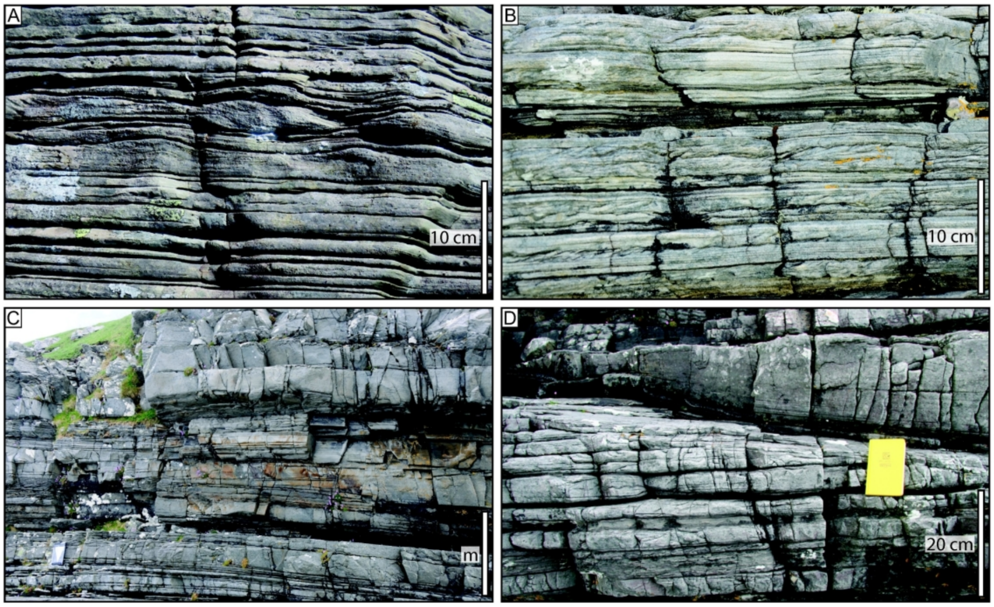

Fig. 9. Plane-laminated fine facies (Facies FL) in FA-4. (A) Thin-bedded, plane-laminated, fine- to medium-grained sandstone with occasional current ripple cross-lamination indicating sediment transport to the right (SW; inferred flood-tide direction) (Glentrosdale Bay South, North Jura; Figs. 1D and 16). (B) Thin-bedded, predominantly plane-laminated medium-grained sandstone, with current ripple cross-lamination and plane-lamination alternating on a scale of 10–30 mm. Note the lack of grading or discrete event beds. Photographed near the base of the coarsening-upward unit in Fig. 18A (Aird Bhreacain, North Jura; Fig. 1D). (C) The lower part of a 6 m-thick coarsening-upward unit, which is mainly composed of well-sorted, fine- to medium-grained, plane-laminated sandstone beds (Aird Bhreacain, North Jura; Fig. 1D). (D) Scoop-shaped erosional surface (dipping left to right), ca 5 m across, with onlapping plane-laminated sandstone, which is characteristic of the lower-to-middle parts of FA-4 coarsening-upward units (Aird Bhreacain, North Jura; Fig. 1D).

169x104mm (300 x 300 DPI)

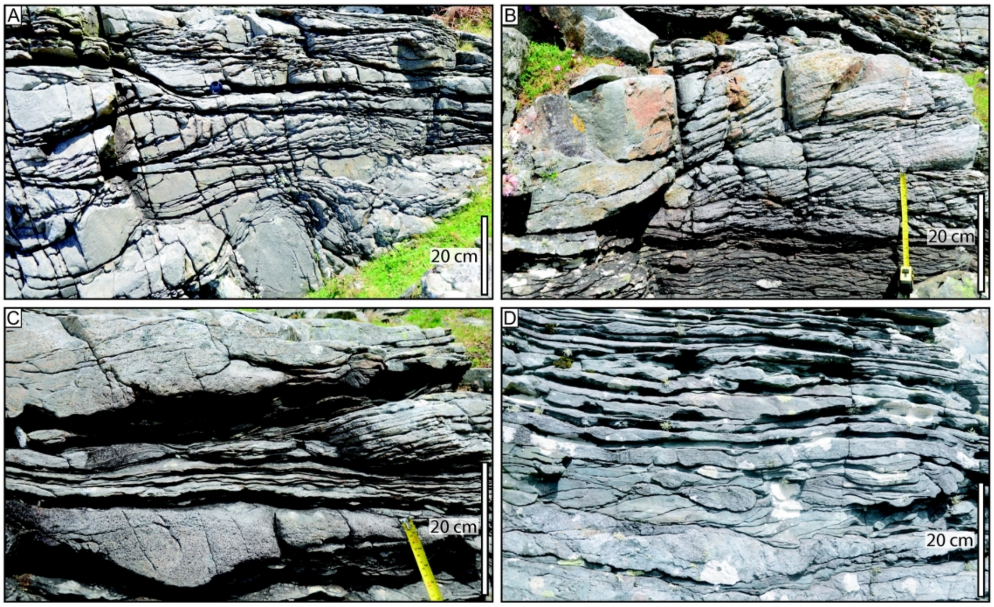

Fig. 10. Heterolithic facies (Facies SH) in FA-5. (A) Cross-bedded, medium- and coarse-grained sandstone with mudstone-draped foresets and mudstone interbeds. Note bed and set amalgamation, long toesets and the thicker toeset mudstone drapes. Interbeds comprise current-rippled, fine- to medium-grained sandstones. (B) Typical amalgamation of sets to form a single 50 cm-thick cross-bed set, which gradually pinches out over ca 5 m to the left (NE; inferred fluvial/ebb-tide direction). (C) Strongly erosional bases to coarse-grained sandstone beds including micro-loading of rippled thin beds. (D) Loaded bed bases to current-rippled sandstone beds, many of which show simultaneous ripple migration and loading, suggesting migration across a soft mud substrate. All four photographs are from Unit 1 of FA-5 in Fig.16, Glentrosdale Bay South, North Jura (Fig. 1D).

169x104mm (300 x 300 DPI)

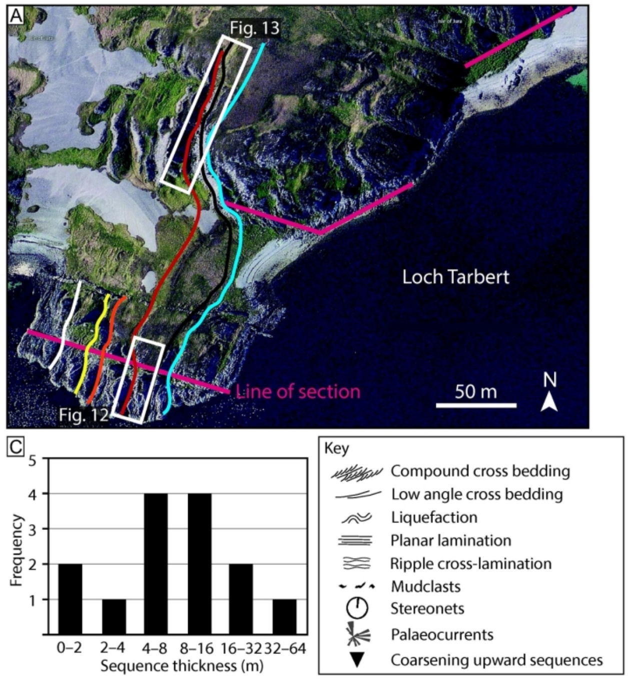

Fig. 11. Stratigraphic stacking patterns and Type 3 erosion surfaces in FA-2 at Aird Reamhar, Central Jura (Fig. 1C). (A) Satellite image (Bing Maps) with the sharp, topographically-defined, periodically-spaced, easterly-dipping Type 3 erosion surfaces (labelled by colours shown in B). The two white boxes define the area of the panoramas in Figs 12 and 13. Palaeocurrent roses, from the intervals between the coloured erosion surfaces, are repeated in those figures. The small circles show the azimuths of isolated paleocurrent observations from other intervals (B) Composite vertical section showing stratigraphic architecture in relation to the Type 3 erosion surfaces (coloured lines), two of which have top-surface winnowed pebble lags (red and pale blue lines at 59 m and 82 m, respectively). The section mostly comprises stacked coarsening-upward units (CU-2b), with a CU-2a unit from 60–73 m (Fig. 12). (C) Spacing of Type 3 surfaces in the logged section.

170x116mm (300 x 300 DPI)

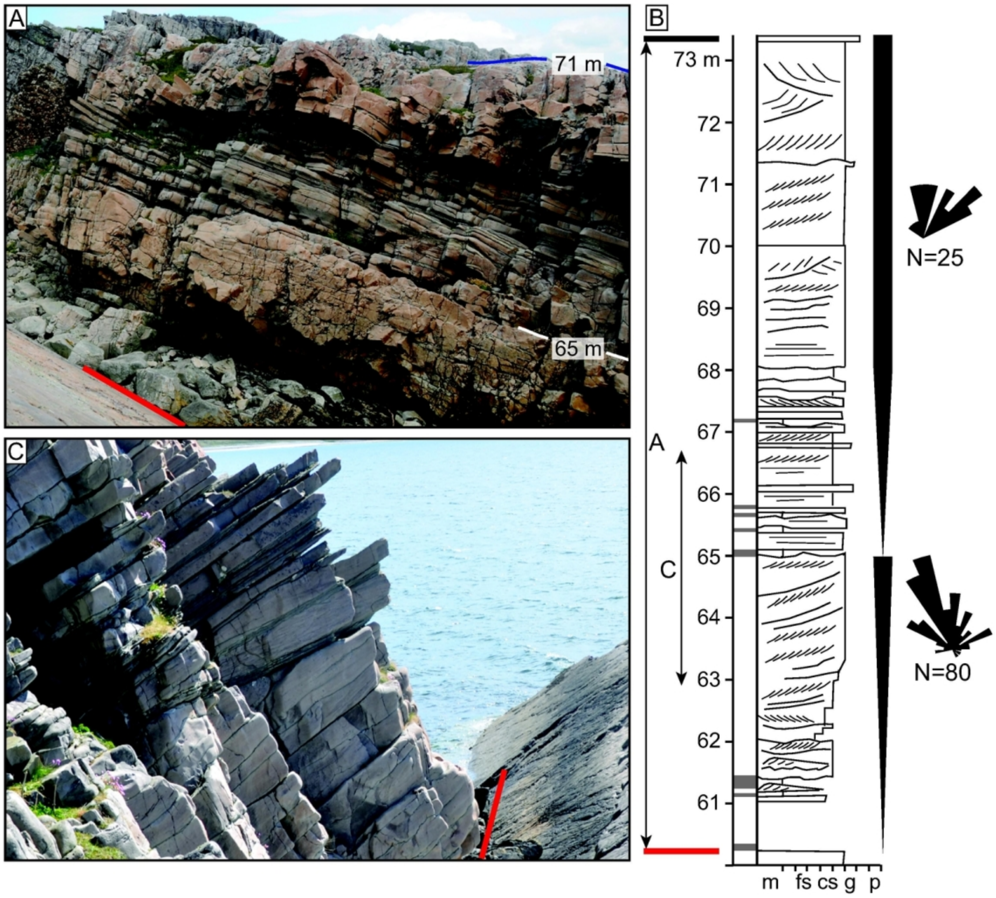

Fig. 12. (A) Photograph of preserved lower section of large-scale bedform in FA-2 at Aird Reamhar, Central Jura (Fig. 1D; 60–73.5 m in Fig. 11B). (B) Stratigraphic log of FA-2 unit shown in Fig. 12A. Overall, the section consists of two coarsening-upward units (CU-2a) between two sharp, planar Type 3 bedding surfaces (red and black as on Fig. 11). (C) The lower part of the section across the boundary between the two successive coarsening-upward units (65m), each commencing with interbedded medium-grained, plane-laminated sandstone and siltstone that passes up into low-angle, plane-laminated medium-grained beds (Facies CS and CL) and dm-scale cross-beds with palaeocurrents towards the NNW. There is a slight counter-clockwise rotation of palaeocurrents between the two component sequences. The upper part of the FA-2 units consists of large-scale cross-bedded, very coarse-grained, occasionally granular, sandstones with superimposed 3–5 m-thick composite sets and dewatering structures. (C) Detailed photograph of lower part of FA-2 unit shown in Fig. 12B.

133x120mm (300 x 300 DPI)

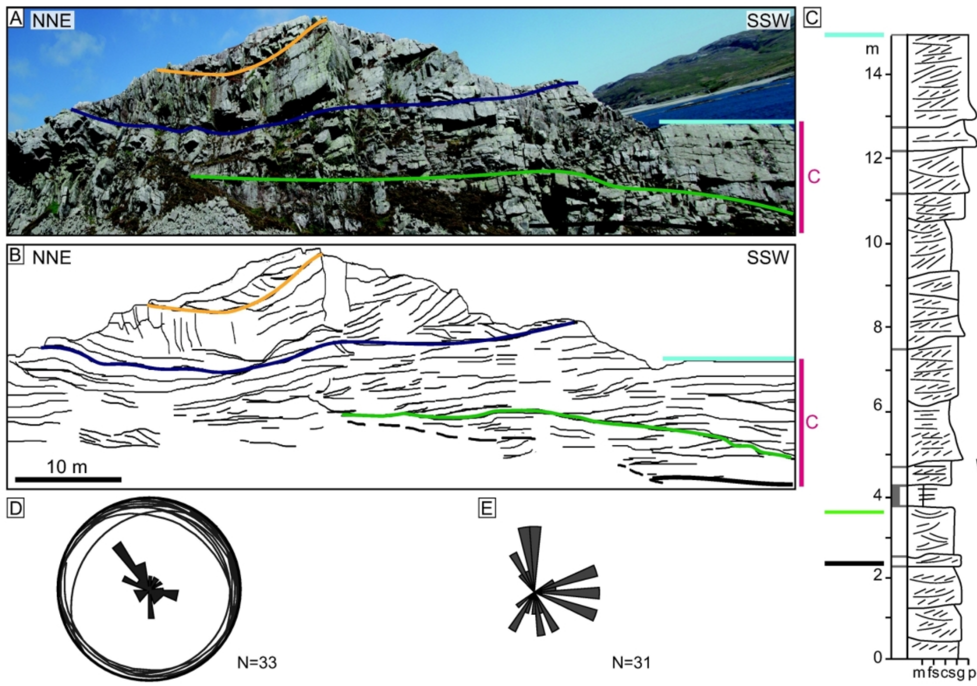

Fig. 13. Bedform migration and erosional geometries in FA-2. The pebble-bearing light blue horizon (in A, B and C) can be correlated as a datum implying that there is 7 m of extra section in this exposure than at the section measured 150 m to the south along the coast (i.e. from 67–81m in Fig. 11B). The exposure photo (A) and sketch (B) are shown with structural dip removed. This shows a downlapping, northward-prograding unit (SSW end of the exposure) above the green surface. A minor coarsening-upward unit (CU-2b) above this downlap surface terminates at a Type 1 bedding surface (5 m in log in C) and is succeeded by cross-bedded coarse-grained sandstone and subordinate interbedded, plane-laminated sandstone. Low-angle surfaces between the green and light blue surfaces have a modal, tilt-corrected, dip of 7° (stereonet in D) and a dominant dip towards the NW (rose diagram in D). Cross-bed dip azimuths from the same interval (E) have a wide dispersion, including some indicating flow lateral to the inclined surfaces. Toward the NNE end of the exposure, the prograding FA-2 units include two nested Type 2 erosion surfaces (black and orange). The black surface passes to the SSW into a non-erosional northward-inclined plane, which downlaps onto the green surface. This suggests that its geometry is due both to constructional relief (SSW) and to erosion (NNE). Aird Reamhar, Central Jura; Fig. 1D.

170x116mm (300 x 300 DPI)

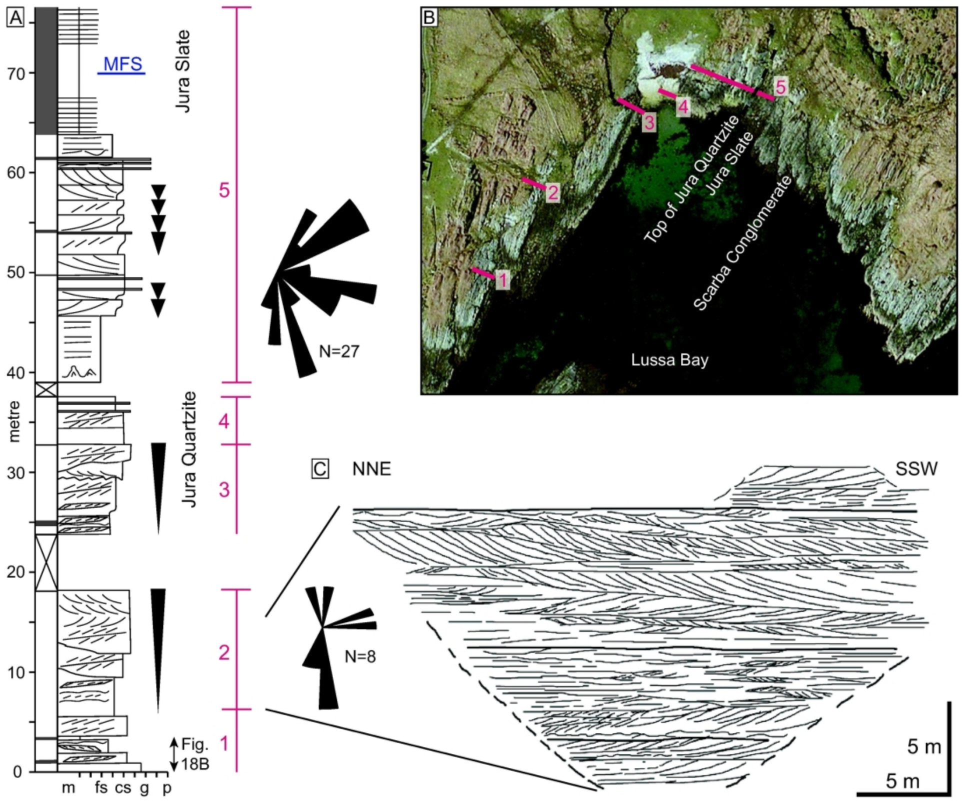

Fig. 14. Heterolithic, dm-scale bedforms in FA-2 in the uppermost Jura Quartzite at Lussagiven, Central Jura (Fig. 1C). Key to sedimentary structures in Fig 11. (A) Sedimentary log with palaeocurrent measurements indicating bimodal ebb- and flood-tide directions. Coarsening-upward units (CU-1, FA-2) with compound sets of heterolithic cross-bedding with mudstone drapes and bidirectional palaeocurrents occur throughout.. The very top of the Jura Quartzite is marked by an unusually large number of small pebble conglomerate lags (e.g. 60–62 m). (B) Satellite image of the logged section, which is a composite of five segments (numbered 1–5) separated by minor faults and gaps with no exposure. Palaeocurent rose diagram in (A) is derived from segemnts 3, 4 and 5 only and that in C from segment 2 (sketched). (C) Exposure sketch of metre-scale, low-angle, concave up cross-bed sets. Palaeocurrent rose diagram (C) indicates variable and oppositely-dipping trends in cm- to m-scale cross-bed sets. This is consistent with preservation of ebb- and flood-tide-influenced sand bars.

170x138mm (300 x 300 DPI)

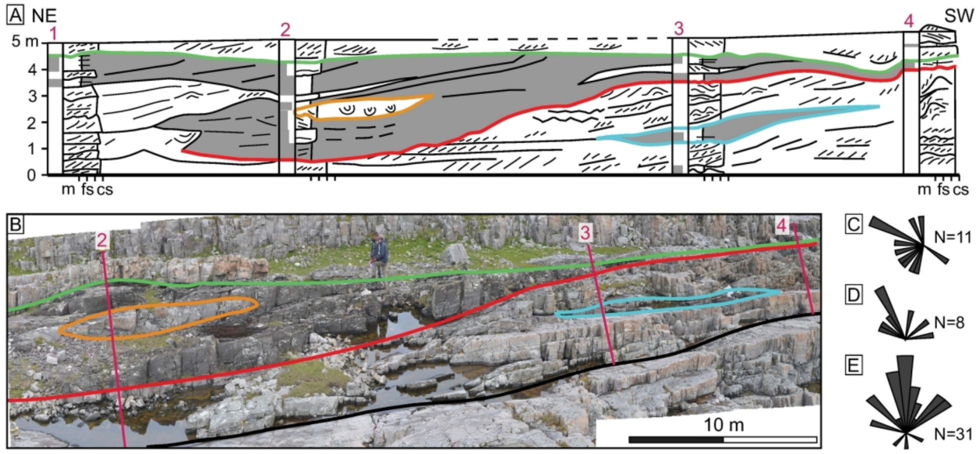

Fig. 15. Large-scale, mudstone-draped, transverse bedform within FA-1. Correlation panel (A) and exposure photograph (B) show inclined bedding planes between two parallel planar surfaces (black below and green above) that define a ca 5 m-high migrating bedform. Palaeocurrent azimuths are measured from superimposed dune cross-bedding (C), which are parallel to the dip direction of the low-angle surfaces (5°), indicating that this was a transverse bedform. Rare reverse palaeocurrents to the SW were measured at the base of the unit. The anomalously thick mudstone-rich unit was possibly deposited as a fluid mud, as evidenced by its massive nature and the sandstone lens (orange) comprising load-balled sandstone. Palaeocurrent patterns from this partly abandoned bedform show bidirectional trends (C). In contrast, palaeocurrent azimuths from laterally adjacent FA-1 sandstones to the South (D) and North (E) of this outcrop, both indicate more unidirectional northerly flow in the inferred active/axial sand-rich transport path (Ruantallain Bothy, Central Jura; Fig. 1C).

169x76mm (300 x 300 DPI)

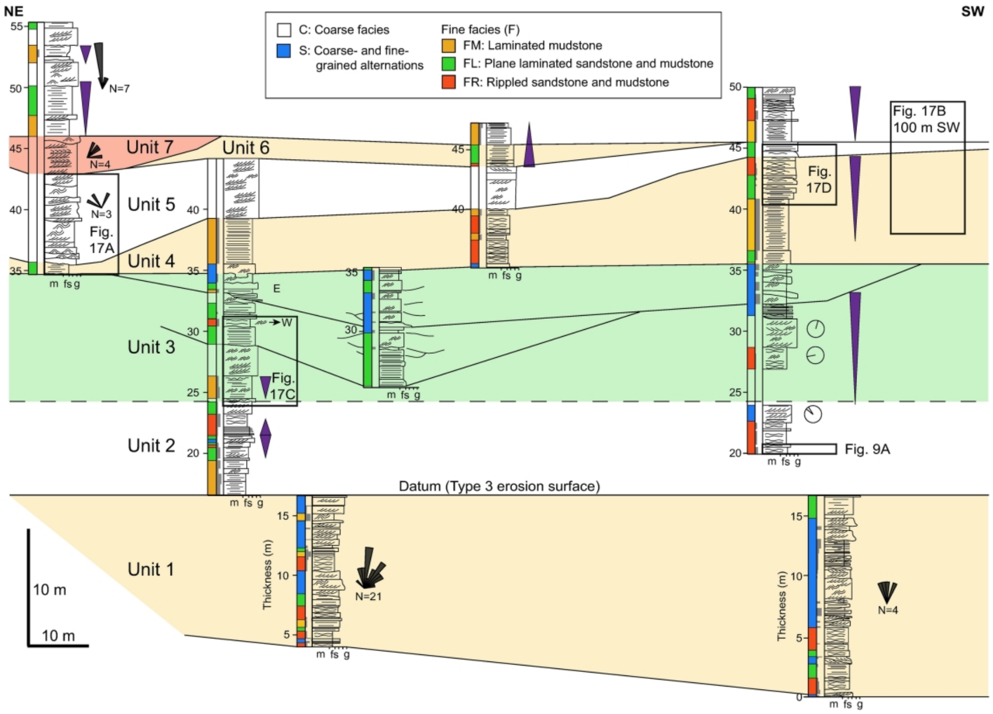

Fig. 16. Vertical and lateral stratigraphic stacking patterns illustrating fluvio-tidal mouth bar facies successions (Glentrosdale Bay South, North Jura; Fig. 1D). Key to sedimentary structures in Fig. 11. Stratigraphic logs span a ca 55 m-thick succession, which extends laterally for ca 150 m. The correlation datum is at the boundary between Units 1 and 2. Beneath this surface, Unit 1 (FA-5) is bounded by two sharp planar Type 3 erosion surfaces, and comprises heterolithic Facies SH and SG, which thicken to the south, implying that either the top or base (more likely the base) is non-horizontal. Unit 2 is fine-grained and comprises thin-bedded sandstone and mudstone of Facies F with both rippled (FR) and plane laminated (FL) beds. A coarsening-upward trend (FA-4) in Unit 3 is vertically and laterally variable, defined by changes from heterolithic deposits (Facies S), through plane-laminated medium-grained sandstone (Facies FL), and into massive liquefied and slumped Facies C. This succession is overlain by local angular unconformities. Unit 4 has a basal planar Type 3 erosion surface and consists of a partially-truncated coarsening-upward unit of plane-laminated sandstone. Note the lateral discontinuity of cross-bedded (blue), rippled (red), versus plane-laminated (green and orange) facies in Units 1–4. These are not stacks of correlatable waning-flow ‘event’ beds. Unit 5 (Facies C, FA-1) is an erosionally-based channel sand that laterally thins and passes gradationally into plane-laminated facies (Facies FL; Fig 17B). Unit 6 closely resembles Unit 4 (FA-4) but is erosionally truncated by Unit 7 (Facies C, FA-1). The facies and stratigraphic geometries of Units 3–7 are interpreted as the deposits of a set of prograding fluvio-tidal distributary channel/mouth bar systems.

229x164mm (300 x 300 DPI)

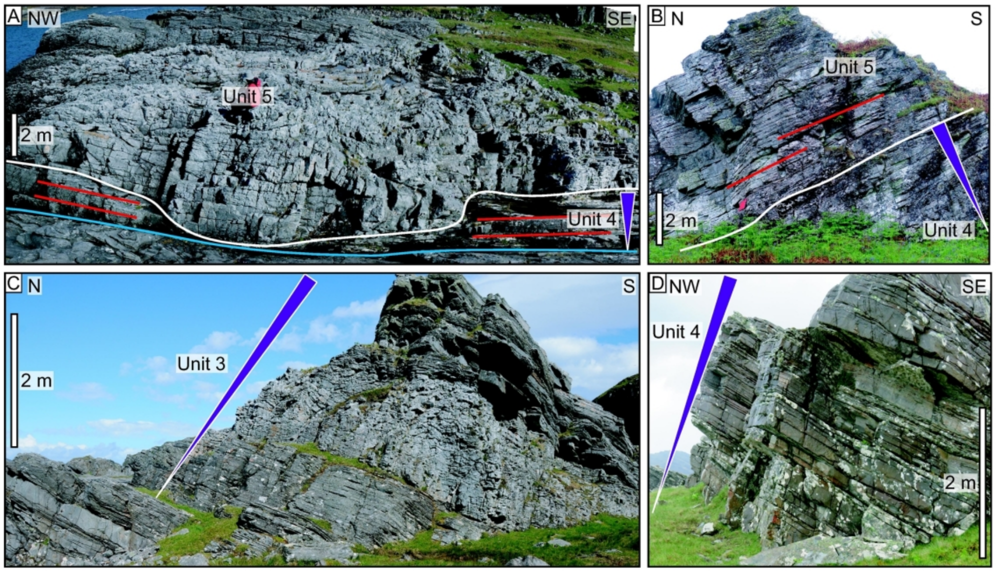

Fig. 17. Stratigraphic architecture of FA-4 at Glentrosdale Bay South, North Jura (Fig. 1D; cf. Fig. 16). (A) Channelised Facies C sandstone (Unit 5) showing erosional incision into the underlying coarsening-upward succession (Unit 4) (see Fig. 16 for equivalent line drawing). (B) Along strike correlative section ca 250 m SW of exposure in A. The white line at the base of the channel is the same as in A and delineates the base of thicker-bedded, plane-laminated, coarse-grained sandstones above the coarsening-upward succession (Unit 4). At this position, the along-strike equivalents of Facies C in channel Unit 7 (Fig. 16) are plane-laminated, medium-grained sandstones (Facies FL) displaying low-angle downlap (red lines). Units 5 and 7 are interpreted as axial channels incising into a laterally-equivalent fluvio-tidal mouth bar. (C) Unit 3 (Fig. 16) comprising the lowermost unit of plane-laminated mudstone and fine-grained sandstones, which coarsens-upward into liquefied and slumped, massive, medium-grained sandstone. (D) Plane-laminated Facies FL in Unit 4, which, to the NE, are incised by Unit 5 (Figs. 16 and 17A).

169x98mm (300 x 300 DPI)

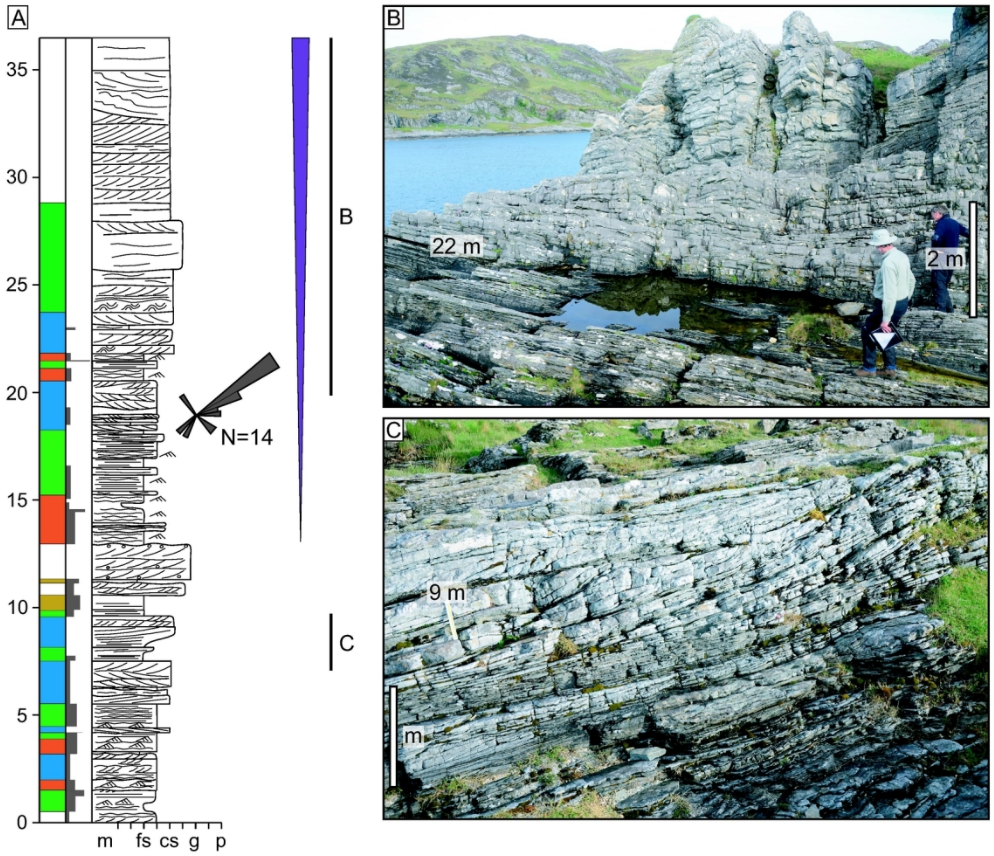

Fig. 18. Stratigraphic architecture and relationships of FA-4 and FA-5 at Aird Bhreacain, North Jura (Fig. 1D). (A) Stratigraphic log with palaeocurrent measurements from Facies S (blue). (B) Exposure photograph of part of the ca 25 m thick coarsening- and thickening-upward unit predominantly consisting of (bottom to top): (1) fine-grained, ripple-cross-laminated sandstones (red in A); (2) plane-laminated thin- to medium-bedded medium-grained sandstone (green in A) with heterolithic cross-bedded facies (blue in A); and (3) liquefied coarse-grained sandstone (Facies C, white in A). (C) Exposure photograph of part of the underlying FA-5 units, predominantly comprising heterolithic facies in the toesets of large-scale bedforms. These facies and stratigraphic characteristics suggest that the FA-4 unit prograded over the FA-5 unit, and are consistent with a fluvio-tidal channel/mouth bar prograding over the toes of a sub-tidal bedform. Facies key as in Fig. 16.

144x124mm (300 x 300 DPI)

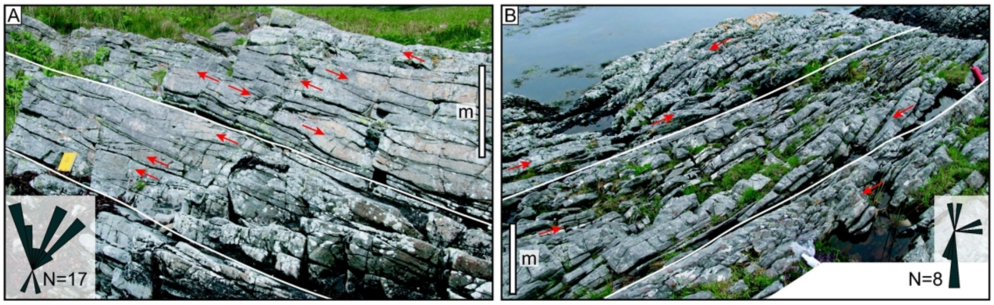

Fig 19. Stratigraphic architecture of FA-5 at Inner Loch Tarbert (A) and Lussagiven (B) (3 m in Fig. 14A), Central Jura (Fig. 1C). Decimetre-thick bedsets of mudstone-draped cross-bed sets are interbedded with plane-laminated and occasionally current ripple cross-laminated thin-bedded sandstones and mudstones. Progradation directions of cross-bed sets (red arrows) display frequent current reversals. Individual units are defined by through-going, metre-scale bedding planes (white). Heterolithic units occasionally form low-angle (5°) compound cosets.

170x53mm (300 x 300 DPI)

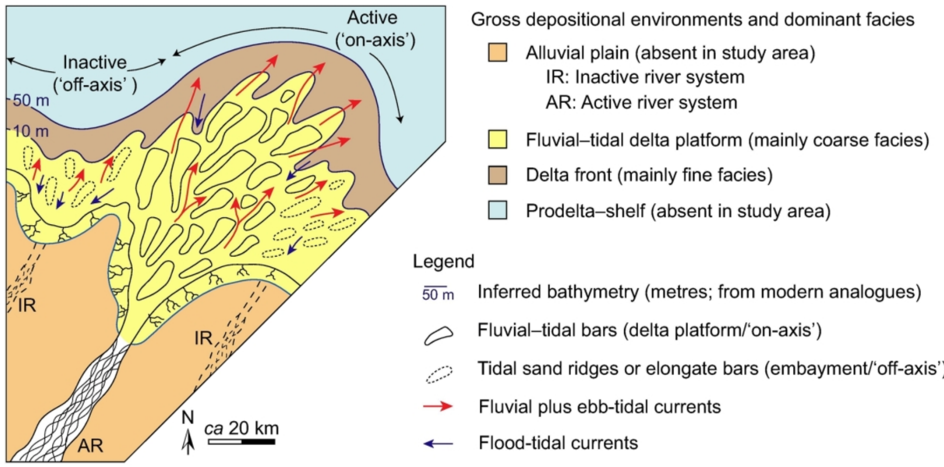

Fig. 20. Depositional model for the Jura Quartzite consisting of a sand-rich fluvio-tidal delta platform dominated by laterally migrating channels with intervening fluvio-tidal bars connected up-depositional-dip to active river systems (AR) ('on-axis'). Lateral embayment areas of decreased sediment supply, adjacent to inactive river systems (IR), include tidal sand ridges or elongate bars ('off-axis') and have more tidal characteristics. Delta progradation and abandonment is largely controlled by upstream avulsion. The predominant coarse facies mostly preserves channel floor deposition that occupies a substantial along transport path extent.

169x81mm (300 x 300 DPI)

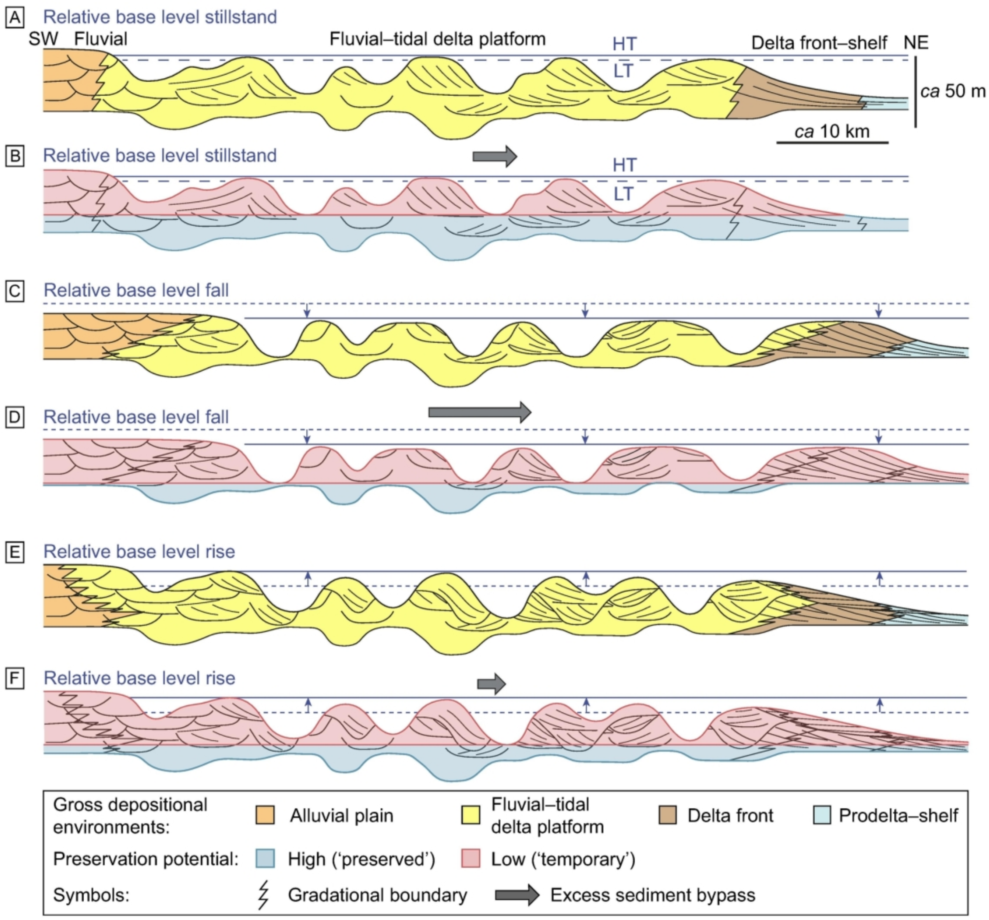

Fig. 21. River-to-shelf cross-sections (approximately 60–70 km NE–SW in the Jura Quartzite), showing high tide (HT) and low tide (LT), and schematic barform morphology and stratigraphy resulting from active channel migration. The lower limit of the cross-sections is an arbitrary 'Regional Composite Scour' surface (Holbrook and Bhattacharya, 2012) that represents erosion by the deepest fluvio-tidal channels (perhaps up to 30–50 m at tidal channel confluences: Ginsberg et al., 2009; Ferrarin et al., 2018). The sections are presented in pairs (A,B), (C,D) and (E,F) with the upper showing facies and the lower preservation potential. (A) The coarse facies (in FA-1,-2,-3 and -5) is in yellow, with inferred proximal alluvial equivalents in orange. The delta-front units (brown) include the predominantly fine facies FA-4 units. The "pro-delta shelf" facies are inferred distal equivalents. (B) As in A but indicating variable preservation potential. The upper limit of high preservation potential (blue) is shown as an arbitrary depth below sea level related to the efficacy of lateral erosion by migrating fluvio-tidal channels, which in reality will vary spatially and temporally. Facies above this level (e.g. bar tops, intertidal deposits, etc.) are selectively removed and are assigned a low preservation potential (red); this sediment is in 'temporary' storage. Excess sediment bypass is indicated by the horizontal grey arrow. (C) As in A but with falling relative base level. Channel incision and increased fluvial gradient increase sediment bypass (grey arrow). There is some mouth bar progradation. (D) As in C but indicating the change in preservation potential related to the relative base level fall. Channel floor deposits are selectively preserved. (E) As in A but with rising relative base level. Sediment bypass is reduced (grey arrow), but an excess of sediment supplied relative to accommodation space is argued for the Jura Quartzite system. The large volume of sediment stored in the fluvio-tidal delta bars provides a 'sediment buffer' whose re-shaping through internal environmental dynamics could, speculatively, counteract transgression-driven facies belt shifts (e.g. Romans et al., 2016). (F) As in E but indicating the change in preservation potential related to the relative base level rise. Channel floor deposits are again selectively preserved, but the preservation boundary aggrades to include shallower bar flanks.

169x156mm (300 x 300 DPI)